

Characterization of CTLA4 trafficking and implications for its function

Sahamoddin Khailaie^{1,2}, Behzad Rowshanravan³, Philippe A. Robert¹, Erin Waters³, Neil Halliday³, Jesus David Badillo Herrera¹, Lucy S. K. Walker³, David M. Sansom^{3,*}, Michael Meyer-Hermann^{1,2,4,*}

¹ Department of Systems Immunology and Braunschweig Integrated Centre of Systems Biology (BRICS), Helmholtz Centre for Infection Research, Braunschweig, Germany.

² Centre for Individualised Infection Medicine (CIIM), Hannover, Germany.

³ Institute of Immunity and Transplantation, University College London and Royal Free Hospital, London, UK.

⁴ Institute for Biochemistry, Biotechnology and Bioinformatics, Technische Universität Braunschweig, Braunschweig, Germany.

* To whom correspondence should be addressed. E-mail: d.sansom@ucl.ac.uk, mmh@theoretical-biology.de

ABSTRACT CTLA4 is an essential negative regulator of T cell immune responses and a key checkpoint regulating autoimmunity and anti-tumour responses. Genetic mutations resulting in quantitative defects in the CTLA4 pathway are also associated with the development of immune dysregulation syndromes in humans. It has been proposed that CTLA4 functions to remove its ligands CD80 and CD86 from opposing cells by a process known as transendocytosis. A quantitative characterization of CTLA4 synthesis, endocytosis, degradation, and recycling and how this affects its function is currently lacking. In a combined *in vitro* and *in silico* study, we developed a mathematical model and identified these trafficking parameters. Our model predicts optimal ligand removal in an intermediate affinity range. The intracellular CTLA4-pool as well as fast internalization, recovery of free CTLA4 from internalized complexes, and recycling are critical for sustained functionality. CD80-CTLA4 interactions are predicted to dominate over CD86-CTLA4. Implications of these findings in the context of control of antigen-presenting-cells by regulatory T cells and of pathologic genetic deficiencies are discussed. The presented mathematical model can be re-used in the community beyond these questions to better understand other trafficking receptors and study the impact of CTLA4 targeting drugs.

Introduction

In a healthy organism, the immune system has to maintain a balance between immune activation and inhibition. For T cells, the decision between these two outcomes is influenced by receptors which are not specific for antigen but provide context for antigen recognition. CD28 and CTLA4 are two such transmembrane receptors expressed by T lymphocytes with opposing stimulatory and inhibitory functions respectively. These receptors bind to the same co-stimulatory ligands, CD80 and CD86, which are expressed by antigen presenting cells (1, 2). While ligation of CD28 with co-stimulatory ligands is essential for full T cell activation and effector functions (3–5), CTLA4 inhibits excess co-stimulation by competing for CD28 ligands and thereby preventing uncontrolled T cell activation and clonal expansion of cells specific for our own tissues. Accordingly, CTLA4 deficiency results in autoimmunity (6–8). Early data suggested that CTLA4 directly inhibits the cells that express it, referred to as the cell-intrinsic pathway of immune inhibition (9, 10). Such cell-intrinsic mechanisms predict that autoimmunity arises in a CTLA4-deficient model due to uncontrolled responses of activated T cells. However, cell-intrinsic inhibition also implies that in a chimeric model, containing a mixture of CTLA4-deficient and CTLA4-sufficient cells, hyperactive CTLA4-deficient cells should still be observed. Surprisingly, a normal immune system with no hyperactivation was found when

this idea was tested experimentally (11–14). This observation suggests CTLA4 may act through a cell-extrinsic mechanism of inhibition where CTLA4 expressing cells exert control on their surroundings. This fits with the demonstration that CTLA4 plays a critical role in regulatory T cells (Treg), an immune cell population with potent cell-extrinsic function (15). Recently, it has been shown that CTLA4 molecules on T cells are able to internalize co-stimulatory molecules from the surface of APCs, by a process known as transendocytosis (16) which, represents a potential mechanism for cell-extrinsic inhibition of T cell activation (17).

Unlike many immune regulatory proteins, CTLA4 molecules are mostly observed intracellularly in cytoplasmic vesicles (18, 19) as a result of their interaction with the $\mu 2$ subunit of the clathrin adaptor protein complex AP2 (20–23). In contrast, CD28 is retained on the plasma membrane (24). The unusual localization of CTLA4 raises questions about how this affects its function. For example, it is not clear how the steady state distribution of CTLA4 molecules results from dynamic trafficking between cytosol and plasma membrane. Various parameters affecting internalization, degradation and recycling rates all have the potential to influence the cellular function. Given the number of parameters that can affect CTLA4 function (eg, trafficking rates, ligand binding affinities, competition between ligands etc.) mathematical models are useful in understanding and predicting the impact of changes in these parameters on CTLA4 suppressive

function. We therefore have derived a mathematical model for *in silico* experimentation in order to test how various parameters can influence CTLA4 function.

In this study, we extract CTLA4 trafficking rates from a series of experimental protocols and corresponding mathematical models in order to understand the behavior of CTLA4 and study its role in ligand clearance. The model shows that cytoplasmic CTLA4 acts as a buffer for CTLA4 surface expression, and boosts ligand uptake at early time-points of ligand exposure. *In silico* ligand uptake experiments suggest that stable CTLA4:ligand binding does not guarantee an efficient ligand uptake, and instead ligand removal is optimally fast for an intermediate affinity range of ligand:CTLA4 interaction. We showed that the process of ligand uptake highly depends on the recycling process, and even expression of a normal amount of total CTLA4 does not guarantee an efficient ligand uptake when the recycling process is impaired. Thus, molecular binding and trafficking properties determine the efficiency of ligand clearance. Furthermore, when CTLA4⁺ cells are exposed to a mixture of natural ligands, we find that CD80 is the dominant competitor, and the uptake of CD86 is highly affected by the presence of CD80, but not vice versa.

Materials and Methods

CTLA4 internalization assay Chinese Hamster (*Cricetulus griseus*) Ovary (CHO) cells, expressing the virally transduced (MP-71 retroviral vector containing) human CTLA4 (UniProtKB accession: CTLA4_HUMAN) were placed in FACS tubes [SARST-EDT] at 1.5×10^6 cell/mL density (150 μ L) before being placed on ice. The cells were washed in 200 μ L PBS- buffer (PBS pH 7.4 [Life Technologies] and 2% w/v Albumine Bovine Serum (BSA) [ACROS Organics]) by spinning cells at 500 g for 5 minutes. The surface CTLA4 was stained using Phycoerythrin (PE) fluorophore-conjugated mouse anti-human CTLA4 antibody (PE-CTLA4) [BD Pharmingen] at 1:100 dilution for 20 minutes on ice. After removing the excess antibody and washing the cells with ice cold PBS-buffer, the cells were placed at 37°C water bath for various duration, allowing CTLA4 internalization from the CHO cell surface, before being placed on ice and fixed with 3% (v/v) paraformaldehyde (PFA) [Agar Scientific] for 15 minutes. The cells were washed and the surface CTLA4 was stained with the Alexa Fluor 647 conjugated chicken anti-mouse secondary antibody [ThermoFisher Scientific] at 1:1000 dilution for 30 minutes on ice before being washed and run through BD LSRFortessa (5L SORP) flow cytometer using yellow-green 561nm (586/15 band pass filter) and red 640nm (670/14 band pass filter) lasers for PE and Alexa Fluor 647 fluorophores, respectively. The data were recorded using BD FACSDiva Software (Version 6.2) and the emission spectra compensated mean fluorescence intensity (MFI) of each fluorophore was obtained using FlowJo 10.0.8r1 software.

CTLA4 molecular counting Quantum Simply Cellular anti-Mouse IgG kit [Bangs Laboratories, Inc.] were used according to the manufacturer's instructions in order to quantify the number of virally transduced human CTLA4 expressed in CHO cells. Briefly,

beads 1-4, which are of known size and antibody binding capacity, were stained with varying amounts of PE-CTLA4 for 30 minutes on ice. The beads were washed in media (DMEM [Life Technologies], 10% FBS [Labtech], 2 mM L-Glutamine [Life Technologies], 1x Penicillin-Streptomycin [Life Technologies]) by spinning at 1060 g for 5 minutes before their median fluorescence intensity (MFI) were obtained using BD LSRFortessa flow cytometer using the yellow-green 561nm (586/15 band pass filter) laser at a set voltage. Bead saturation levels with PE-CTLA4 antibody were assessed using the FlowJo 10.0.8r1 software and the best MFI for each bead was plotted in order to establish a calibration curve. In parallel to the above, various number of CHO cells expressing human CTLA4 were fixed with 3% (v/v) PFA [Agar Scientific] for 15 minutes on ice before being washed in media and permeabilised with 0.1% (v/v) saponin in media. The cells were then stained in an identical manner to the beads and ran through BD LSRFortessa flow cytometer using identical settings and voltages as the beads. The obtained CHO cell MFIs were then compared against the calibration curve in order to obtain the number of CTLA4 molecules per CHO cell.

Synthesis-block assay CHO cells expressing CTLA4 were placed in a 96-well U bottom plate [Falcon] at 2×10^6 cell/mL (130 L) before adding cycloheximide at 50 ng/mL or DMSO vehicle control for the indicated times. The cells were fixed as described before then permeabilised in 150 μ L PBS+ (PBS, BSA, 0.1% saponin) for 10 minutes at room temperature before being stained with BNI3 clone PE-CTLA4 antibody as described before. After removing the excess antibody and washing the cells with ice cold PBS+ twice, they were re-suspended in PBS and run on flow cytometer and analysed as described before.

Lysosomal-block assay A total of 1.5×10^5 cells per condition were plated in a 96-well plate and pulsed with anti-CTLA4-PE (BNI3) for 1 hour at 37°C. Cells were then washed twice, and resuspended in medium containing DMSO or NH₄Cl for 2, 4 or 6 hours. At each time point, cells were transferred to FACS tubes and fixed in 2% paraformaldehyde (PFA) on ice for 10 minutes. Cells were then washed 3 times in PBS and analysed for CTLA4 expression by flow cytometry.

All the experiments were performed in triplicates and the MFI values were averaged from 10000 cells (events) for each repeat.

Mathematical models Different mathematical models were developed according to the experimental protocols. Models were studied analytically and numerical simulations were performed by C++ (Boost.Numeric.Odeint) and MATLAB. A differential evolution algorithm was implemented in C++ for parameters estimation. Markov chain Monte Carlo (MCMC) analysis was performed in MATLAB. The mathematical analysis is described in the *Supporting Material (SM)*.

Results

Generation of the model

The rates of CTLA4 internalization, recycling and degradation were estimated from a series of *in vitro* experiments in

which the individual processes of CTLA4 trafficking were perturbed. These experiments were replicated by generating corresponding mathematical models. The parameters of the model were determined by simultaneously fitting all parameters to all experimental results with a combined cost function, using differential evolution algorithm (see *SM - Parameter estimation*). To examine the impact of the experimental data variations on the estimated parameters, we employed MCMC approach to obtain the distribution of the parameters (see *SM - Markov chain Monte Carlo analysis*). The optimal values of the CTLA4 trafficking rates obtained by the differential evolution are within the 68%-confidence interval of their distributions. We, therefore, used the optimal values of the parameters in our simulations. The experimental data used in this study were sufficient to determine all of the CTLA4 trafficking parameters and their distributions given in Table 1. While the parameters were identified using data from all experiments, for the purpose of clarity, the different experiments informing the model are presented individually below, together with their respective mathematical model.

CTLA4 trafficking in the absence of ligands

Following synthesis, CTLA4 is transported from the Golgi to the cell surface. This transport is dependent on the enzymes phospholipase D and ADP ribosylation factor 1 (25) and occurs via the fusion of CTLA4-containing vesicles with the plasma membrane. Surface-expressed CTLA4 is then subject to constitutive endocytosis, independent of ligand binding, via interaction of the tyrosine-based motif (YVKM) in the CTLA4 cytoplasmic domain with clathrin adaptor complex AP2 (20–23, 26). Following internalization CTLA4 molecules can be recycled to the plasma membrane or degraded in lysosomal compartments (24, 27, 28). These features of CTLA4 behavior are seen in primary human T cells and are preserved in model systems transfected with CTLA4 (26).

Based on the above biological observations, we constructed a trafficking model, which comprises processes of protein synthesis, recycling, internalization and degradation. This model, depicted schematically in Fig. 1A, relies on the following assumptions: CTLA4 molecules are synthesized by a constant rate σ_i . Newly synthesized CTLA4 molecules are incorporated to the plasma membrane ($R_p(t)$) and subsequently internalized into the cytoplasm ($R_c(t)$) with rate k_i . This assumes that newly synthesized CTLA4 molecules do not directly undergo degradation in the cytoplasm, but only after endocytosis. Cytoplasmic CTLA4 molecules are degraded in lysosomal and nonlysosomal pathways with constant rates δ_l and δ_n , respectively. Therefore, the total cytoplasmic degradation rate is $\delta_c = \delta_l + \delta_n$. Non-degraded cytoplasmic CTLA4 molecules are recycled to the plasma membrane with constant rate k_r . All variables and parameters represent the value for a single cell (per cell). Such a trafficking model can be repre-

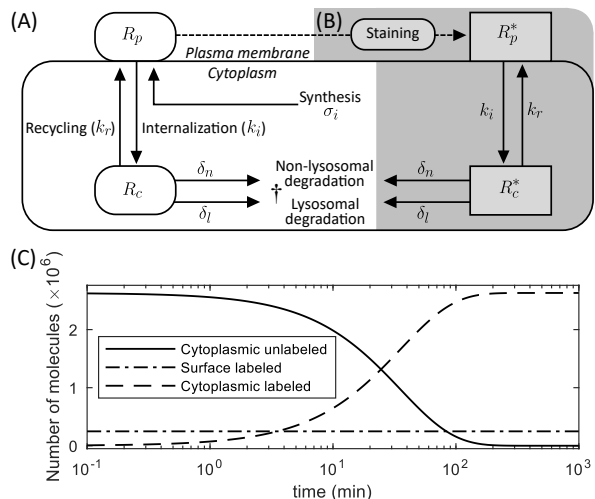


Fig. 1. Ligand-independent CTLA4 trafficking and CTLA4 staining models. (A) Natural trafficking of CTLA4 molecules. The corresponding ODE-based model is given in Eq. S1. (B) By extracellular CTLA4 staining with antibody, the CTLA4 pool is segregated into labeled (shown with grey background) and unlabeled pools. This is a simplified model of a more complex staining model described in *SM - CTLA4 staining model* and shown in Fig. S1. (C) CTLA4 staining simulation. Eq. S12 was solved analytically and the solution, given in Eq. S13, was plotted.

sented by the ordinary differential equations (ODE), given in Eq. S1 (see *SM - Ligand-free trafficking model of CTLA4*).

To recapitulate the experimental observation that CTLA4 molecules are mostly located in the cytoplasm, the model in its steady state (ss) condition has to satisfy the condition $k_i > k_r + \delta_c$ (see Eq. S2, with condition $R_{p,ss}/R_{c,ss} < 1$). Despite the dependence of steady state total CTLA4 values on the rate of protein synthesis, the ratio of surface to cytoplasmic CTLA4 is independent of the level of synthesis (Eq. S2). Further, the steady state absolute number of the cytoplasmic CTLA4 molecules is independent of the rates of internalization and recycling (Eq. S2).

To inform our model, initial parameter estimates were determined using a variety of different antibody staining protocols. By staining CTLA4 with specific fluorescent antibodies at 4°C it is assumed that all surface molecules present on the plasma membrane are labeled at a particular time point. Subsequently, trafficking of CTLA4 is controlled by changes in the temperature where 37°C permits internalization and recycling of CTLA4 not seen at 4°C. In order to label a subset of the cytoplasmic CTLA4, staining was performed at 37°C for a certain duration, after which the kinetic of labeled CTLA4 could be observed. These basic principles were used in various ways to monitor internalization, recycling and degradation of CTLA4 molecules. The general mathematical model for the dynamics of CTLA4 staining is described in *SM - CTLA4 staining model* (see Fig. S1 and Eq. S3). The staining model is simplified based on the following assumptions:

Table 1: Ligand-independent CTLA4 trafficking parameters

Parameter	Description	Dimension	Optimal value ^a	Posterior mean \pm standard deviation ^b
σ_i	Rate of CTLA4 synthesis	# min ⁻¹	10100 ^c	13414 \pm 6936
k_i	Rate of CTLA4 internalization	min ⁻¹	0.2988	0.379 \pm 0.116
k_r	Rate of CTLA4 recycling	min ⁻¹	0.0243	0.028 \pm 0.012
δ_n	Rate of nonlysosomal degradation	min ⁻¹	0.0014	0.0016 \pm 0.00057
δ_l	Rate of lysosomal degradation	min ⁻¹	0.0024	0.0035 \pm 0.0014
δ_c	Rate of cytoplasmic degradation	min ⁻¹	$\delta_l + \delta_n$	0.0051 \pm 0.0015

^a Optimal values were obtained by differential evolution algorithm. See *SM - Parameter estimation*.

^b Parameter distributions were obtained by MCMC analysis. See *SM - Markov chain Monte Carlo analysis*.

^c See *SM - Estimating the rate of protein synthesis*. This value represents the rate of CTLA4 synthesis of cell line used for the molecular counting experiment.

(A) the concentration of staining antibodies in the medium is sufficiently large and does not drop as a result of target binding (thermic bath approximation), (B) staining antibodies bind to CTLA4 molecules with a higher rate than the rate of trafficking processes (quasi steady-state approximation), (C) staining antibodies remain bound to CTLA4 molecules during the time of sample observation (negligible unbinding rate), and (D) staining antibodies do not alter the natural trafficking of CTLA4 molecules and associated rates. The simplified model is shown in Fig. 1A-B, where R_p^* and R_c^* are the numbers of labeled CTLA4 molecules on the cell surface and in the cytoplasm, respectively. The corresponding ODEs are given in Eq. S12 (see *SM - Reduction of the CTLA4 staining model*). Note that in the simplified staining model, the number of unlabeled surface CTLA4 during the staining is zero, because all free surface CTLA4 molecules are labeled instantly when exposed to staining antibodies in the medium (assumption B). Before starting the staining experiment, the number of CTLA4 molecules is assumed at equilibrium (Eq. S2). During the staining process at 37°C, the unlabeled pool of cytosolic CTLA4 molecules becomes exhausted with a half-life of $t_{1/2} = \ln(2)/(k_r + \delta_c) \approx 25$ minutes as a result of transport to the plasma membrane and subsequent labeling, as well as cytosolic degradation (see Eq. S13a). Therefore, the rates of recycling and degradation dictate the duration of the staining process required to label the majority of total cellular CTLA4 molecules.

The dynamics of the different pools of CTLA4 molecules during persistent staining is shown in Fig. 1C. Due to instant labeling of surface molecules as well as continued exocytosis of newly synthesized CTLA4, the number of labeled CTLA4 molecules on the cell surface starts and remains at its equilibrium value whereas unlabeled cytoplasmic CTLA4 molecules become exhausted over time.

CTLA4 internalization

To observe the internalization of surface CTLA4 molecules, we used a CTLA4 internalization assay described in *Materials and methods*. In this experiment, CTLA4-expressing

cells were labeled at 4°C with a fluorescently conjugated anti-CTLA4 antibody (PE-CTLA4). Excess antibody was washed off and the temperature raised to 37°C for various durations to permit CTLA4 trafficking. After this period, a secondary antibody (Alexa fluor 647) was applied at 4°C to detect the remaining surface antibody-labelled CTLA4. In this setting, the initial amount of surface CTLA4 is quantified by PE and the number of molecules still at the surface after a period of trafficking is quantified by Alexa 647. The data of this experiment are shown in Fig. 2A.

In the model, the number of surface CTLA4 molecules before starting the staining process is derived from the steady state solution of the CTLA4 trafficking model, given in Eq. S2. This number is assumed to be fully labeled on ice at $t=0$, leaving no unlabeled molecules on the cell surface. The solution of the dynamic equations provides the time course of the number of CTLA4 molecules in different pools (see *SM-CTLA4 internalization model*, Eq. S15). Surface labeled CTLA4 molecules vanish over time monotonically, becoming cytoplasmic due to internalization (Fig. 2B), while the cytoplasmic labeled CTLA4 pool diminishes after a transient increase due to degradation. Newly synthesized and recycled unlabeled CTLA4 molecules replace the labeled pool over time.

An *in silico* internalization experiment in which CTLA4 synthesis is stopped ($\sigma_i = 0$) predicts that unlabeled CTLA4 molecules on the plasma membrane are cleared after transient maintenance at 76% of its pre-experiment (normal steady state) value (see Fig. 2C) resulting from the utilisation of the cytoplasmic CTLA4 pool. This suggests that without new CTLA4 synthesis, CTLA4 stored in the cytoplasm can temporarily buffer surface CTLA4 expression.

Modeling perturbations of the CTLA4 steady state

CTLA4 synthesis is key for longterm maintenance of surface expression Quantification of the contribution of protein synthesis to CTLA4 homeostasis was based on the synthesis-block experiment (see *Materials and Methods*) in

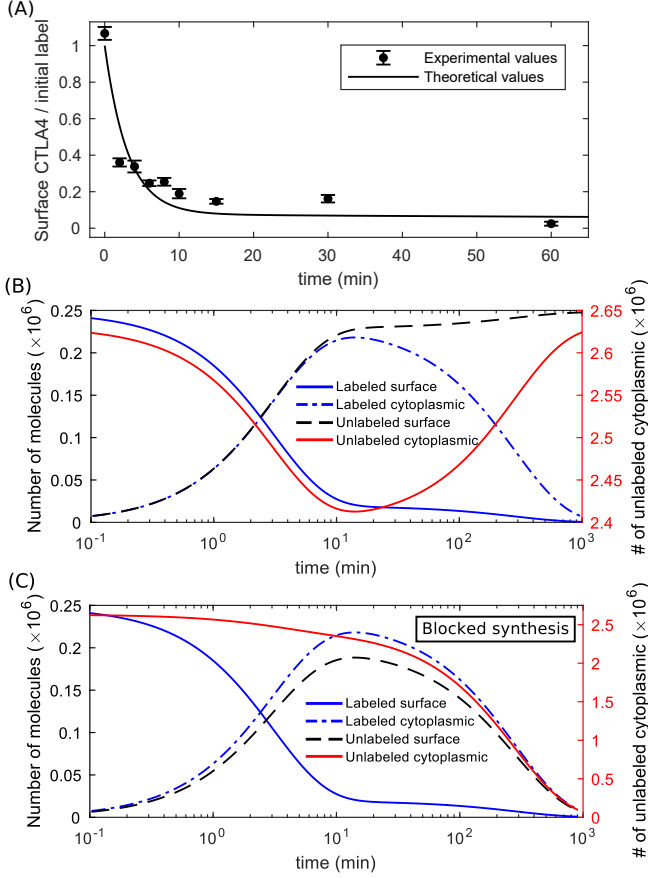


Fig. 2. *In silico* and *in vitro* internalization data. (A) The fraction of initially labeled CTLA4 molecules detected on the cell surface over time is shown. Experimental data points are scaled with the factor $1/S_{\text{int}}$ (see Table S1). (B) The kinetics of all different CTLA4 pools in the model. Unlabeled CTLA4 follows Eq. S1. Unlabeled cytoplasmic CTLA4 molecules ($R_c(t)$) drop transiently (right y-axis). (C) An *in silico* internalization experiment with a block of CTLA4 synthesis. Both unlabeled CTLA4 pools clear over time; however, the surface unlabeled pool transiently reaches 76% of its steady state value in normal cells.

which CTLA4-expressing cells were treated with Cycloheximide (CHX) for different durations, the total number of CTLA4 molecules was measured and compared with cells without CHX treatment.

In the model, we assume that CHX treatment of cells completely blocks protein synthesis ($\sigma_i = 0$). The time evolution of surface and cytoplasmic CTLA4 in the presence of CHX is calculated (see *SM - Block of CTLA4 synthesis model*, Eq. S18) and depicted in Fig. 3A. At early time points, surface CTLA4 is quickly lost due to fast internalization and recycling partially compensates surface CTLA4 loss. Total CTLA4 reduces by degradation in the cytoplasm.

When the CTLA4 synthesis is blocked ($\sigma_i = 0$) and the remaining processes (internalization, recycling and cytosolic degradation) are included (see Fig. 3A), the surface, cytoplasmic

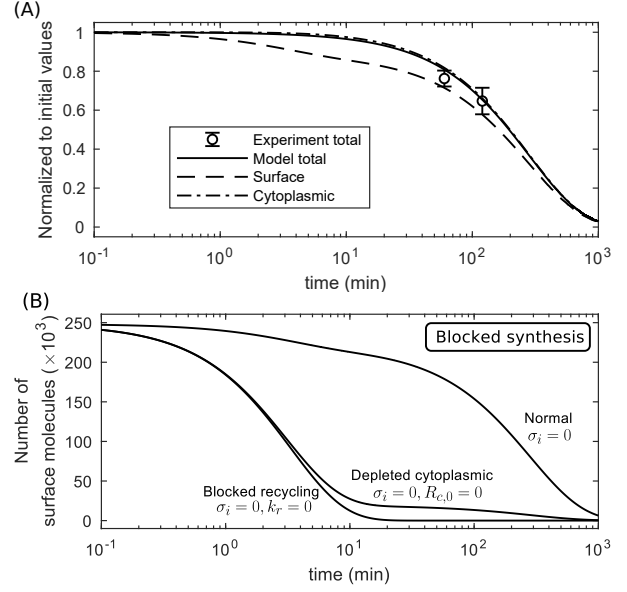


Fig. 3. Block of CTLA4 synthesis. (A) A single experimental data point was compared to the theoretical value in Eq. S21. CTLA4 molecules in the cytoplasm can transiently compensate CTLA4 loss on the plasma membrane after the block of synthesis. However, both pools become exhausted with extended exposure to CHX. (B) *In silico* experiment of blocked synthesis with additional depletion of cytoplasmic CTLA4 ($R_{c,0} = 0$) or block of recycling ($k_r = 0$). These curves are obtained by numerical solution of the trafficking model in Eq. S1. In the absence of cytoplasmic CTLA4 or of the recycling process, the surface CTLA4 clears quickly, reducing by 50% within ≈ 2.41 and 2.32 minutes, respectively.

mic and total CTLA4 molecules are reduced by 50% within 160, 198 and 195 minutes, respectively. Surface CTLA4 is reduced by 8% within 3 minutes while cytoplasmic CTLA4 only by 0.4% during this time, which indicates a rapid loss of surface CTLA4 at early time-points. As expected, CTLA4 synthesis is important for maintaining the homeostatic number of CTLA4 molecules.

Next, we addressed the contribution of the cytoplasmic pool to ask how internalization impacts CTLA4 surface expression. In an *in silico* experiment, a complete depletion of the cytoplasmic CTLA4 (by imposing a zero initial value, $R_{c,0} = 0$) or a complete block of recycling ($k_r = 0$) were tested, in the absence of CTLA4 synthesis. This showed that surface CTLA4 molecules clear within a few minutes in comparison to the half-life of 160 minutes under normal condition ($\sigma_i = 0$) (see Fig. 3B). The model predicts that in the absence of new synthesis, CTLA4 can be maintained at the cell surface by recycling. Thus, the cytoplasmic reserves of CTLA4 molecules are key for maintaining the surface CTLA4 pool.

Lysosomal dominates nonlysosomal degradation To quantify the impact of lysosomal degradation on CTLA4 trafficking, we used the lysosomal-block assay in which

CTLA4 kinetics were measured in presence or absence of ammonium chloride (NH_4Cl) (see *Materials and Methods*). NH_4Cl inhibits lysosomal degradation through lysosomal pH neutralization. In this experiment, cells were initially pulsed with a labeling antibody (anti-CTLA4 PE) at 37°C for 60 minutes. After washing, degradation of CTLA4 molecules was quantified by flow cytometry (see Fig. 4A).

To reconstruct this experiment *in silico*, we used the staining model (Fig. 1A-B) and calculated the number of labeled CTLA4 molecules after 60 minutes. Starting from this value as initial condition, the time evolution of the CTLA4 pools was calculated (see *SM - Block of lysosomal degradation*, Eq. S22) in the presence (+) or absence (-) of NH_4Cl . It was assumed that NH_4Cl does not impact on the nonlysosomal degradation pathway. A comparison of both conditions reveals the differences in the kinetics of CTLA4 molecules (see Fig. 4B): After the initial decrease of the number of unlabeled CTLA4 molecules during the staining step, it increases to its steady state value or higher in the absence or presence of the lysosomal inhibitor, respectively. This increase is due to ongoing CTLA4 synthesis. The rate of degradation decreased by $\approx 63\%$ and the half-life of total labeled CTLA4 molecules increases from approximately 3.3 hours to 8.8 hours in the presence of the lysosomal inhibitor (see Fig. 4A). The model predicts that the lysosomal degradation pathway is dominant.

According to the steady state number of CTLA4 molecules in the CTLA4 trafficking model Fig. 1A (see $R_{p,ss}/R_{c,ss}$ in Eq. S2), reduction of the cytoplasmic degradation (δ_c) leads to a reduction in the fraction of the total CTLA4 molecules that appears on the cell surface.

These results suggest that the lysosomal degradation of CTLA4 is a fast process, regulates the homeostatic number of CTLA4 molecules, and, when blocked, shifts the steady state subcellular distribution of CTLA4 towards the cytoplasm.

CTLA4 recycling is slower than internalization For quantification of CTLA4 recycling, we used a two-step staining protocol to label CTLA4 molecules on the plasma membrane, allow them to internalize and then to label molecules upon their return to the surface (26). In the first step, CTLA4-expressing cells were incubated with Alexa488-conjugated anti-CTLA4 (a green antibody) for 60 minutes at 37°C . Then, cells were washed and surface CTLA4 molecules were blocked at 4°C with unconjugated anti-human IgG, a secondary antibody without any color. This prevented those molecules that remained on the surface and were green-labeled from binding to a secondary antibody. After washing, cells were incubated for different times with Alexa555-conjugated anti-human IgG (a red secondary antibody) at 37°C . The red antibody only binds those green-labeled CTLA4 molecules that recycled back to the plasma membrane. The red-fluorescent intensity was quantified with confocal microscopy reflecting the time evolution of the labeled subset of recycled CTLA4. Experimental data are taken from

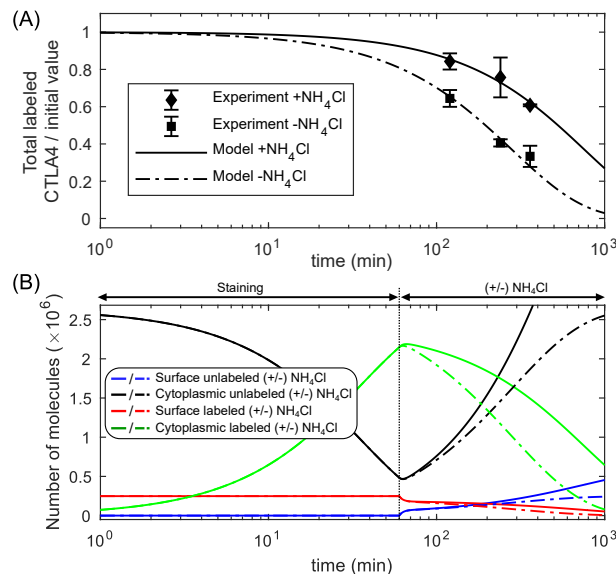


Fig. 4. Block of lysosomal-degradation. (A) *In silico* versus *in vitro* results with and without addition of NH_4Cl . (B) *In silico* prediction of different CTLA4 pools for blocked lysosomal degradation (+ NH_4Cl , solid lines) and normal condition (- NH_4Cl , dash-dotted lines).

(26) and shown in Fig. 5A.

The corresponding *in silico* experiment replicates the two staining steps. At first, the number of green-labeled CTLA4 molecules stained on the cell surface and subsequently internalized within 60 minutes is calculated from the staining model in Fig. 1A-B. During the CTLA4 block on ice, we assumed that all green-labeled molecules on the cell surface are blocked (denoted by green-blocked in Fig. 5B)), and undergo natural trafficking at normal temperature. In the model, application of the red secondary antibody labels only those CTLA4 molecules that recycle back from the cytosol and do not belong to the blocked subset. This defines a green-red labeled pool of molecules (see *SM - CTLA4 recycling model*).

According to the modeling results (Fig. 5B), in the second staining step, green-blocked molecules clear monotonically from the cell surface by internalization, while the green-blocked cytoplasmic molecules vanish after a transient increase, reaching 88% of total initially blocked CTLA4 molecules after 14 minutes ($t=74$ minutes) of trafficking. Such a transient increase is also observable for green-red labeled molecules, which originate from the green-labeled cytoplasmic pool. The number of green-red labeled molecules on the cell surface reaches its maximum value (at $t=74$ minutes) faster than the cytoplasmic pool (at $t=147$ minutes), since the labeling is only possible by passing through the cell surface first. The green- and red-labeled CTLA4 molecules clear over time and are replaced with the unlabeled CTLA4 molecules.

In an *in silico* recycling experiment, in which the CTLA4

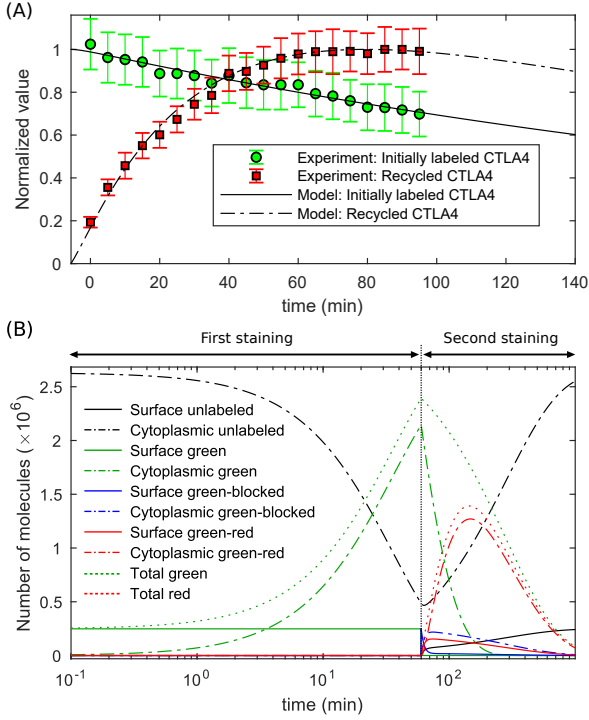


Fig. 5. Recycling experiment and simulation. (A) *In vitro* data taken from (26) and corresponding *in silico* values for the number of green- and red-labeled CTLA4 molecules. (B) Model prediction of different CTLA4 pools during the staining procedures (see Eq. S27). The vertical line at $t=60$ minutes indicates the block of green-labeled CTLA4 and the starting time of the second staining step.

degradation is blocked ($\delta_c = 0$) in the second staining step, the cytoplasmic green-labeled (not blocked) CTLA4 is exclusively cleared by recycling with a predicted half-life of ≈ 28 minutes. These results suggest that recycling of the cytoplasmic CTLA4 occurs rapidly, but significantly slower than internalization ($t_{1/2} = \ln(2)/k_i = 2.32$ minutes, see Fig. 3B).

Biological Implications

In the previous section, all parameters of the model have been identified by experimental constraints in a simultaneous fitting to all staining experiments. In the following the model is evaluated and used to generate predictions on CTLA4 dynamics and functionality.

The subcellular CTLA4 distribution is not altered by CTLA4 synthesis Since regulatory T cells are known to upregulate CTLA4 synthesis upon TCR ligation, we investigated how altering this parameter in the model impacted on CTLA4 cellular distribution. The ratio of surface to cytoplasmic CTLA4 in steady state condition is independent of the rate of CTLA4 synthesis (see Eq. S2). However, by changing synthesis, the trafficking model deviates from its equilibrium

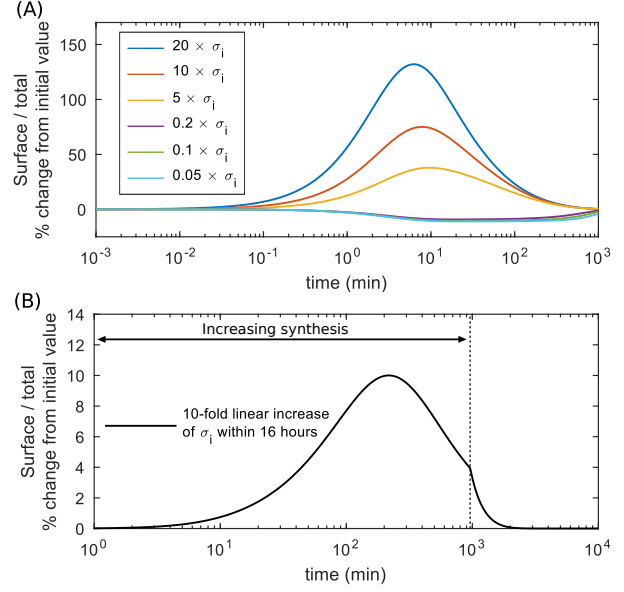


Fig. 6. CTLA4 subcellular distribution transiently changes upon variation of CTLA4 synthesis. The rate of protein synthesis (σ_i) is varied (A) sharply and (B) smoothly from its original value, and the dynamic change of the fraction of CTLA4 molecules expressed on the cell surface ($R_p(t)/(R_p(t) + R_c(t))$) is calculated. After a transient change, the fraction converges to its original (steady state) value $(k_r + \delta_c)/(k_i + k_r + \delta_c)$. Deviation (%) of the fraction from its steady state value is shown.

state, and the absolute number of CTLA4 molecules changes to a new steady state value. This transition induces a transient change in the subcellular distribution of CTLA4. By increasing or decreasing the rate of CTLA4 synthesis, the fraction of CTLA4 molecules on the cell surface transiently increases or decreases, respectively but returning to the steady state distributions over time. Fig. 6A shows how a sharp change in the rate of protein synthesis transiently deviates the subcellular distribution whereas smooth change in the rate of protein synthesis has less impact on the distribution of CTLA4 molecules (Fig. 6B). Given the fact that CTLA4 upregulation can be of the order of 10-fold within 12 hours (29), these results suggest that the subcellular distribution of CTLA4 is only subtly altered by upregulation of CTLA4 synthesis.

High affinity ligands exhaust cytosolic CTLA4 The CTLA4 staining model in Fig. 1A-B relies on the assumption that labeling antibodies remain bound to and degrade along with the bound CTLA4 molecules. Theoretically, this is a good approximation for ligands with high affinity (high on-rate and low off-rate) to CTLA4 molecules, such as pharmacological ligands. The rate of ligand removal from the medium to the cytoplasm, in addition to the rate of internalization, also depends on the flow of free (unbound) CTLA4 molecules to the cell surface (F_{cs}), which is provided by CTLA4 synthesis (σ_i) and recycling (with rate k_r) of the free cytoplasmic

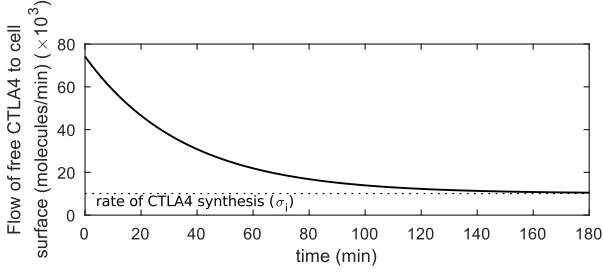


Fig. 7. Flow of free CTLA4 to the cell surface. The flow of free CTLA4 molecules to the cell surface is obtained from Eq. 1. This flow converges to the rate of CTLA4 synthesis by clearing the pool of free cytoplasmic CTLA4 molecules ($R_c(t)$). The analytic function of $R_c(t)$ is given in Eq. S13a.

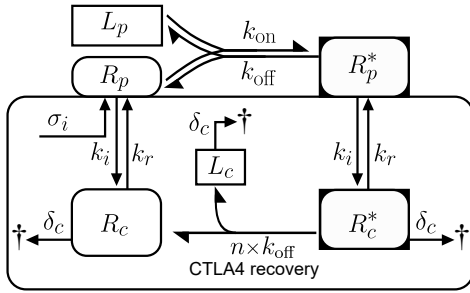


Fig. 8. Scheme of binding reaction and CTLA4 trafficking for limited extracellular ligand concentration. The corresponding mathematical model is given in Eq. S35.

CTLA4 molecules ($R_c(t)$)

$$F_{cs}(t) = \sigma_i + k_r R_c(t). \quad (1)$$

Upon exposure to high affinity ligands, the free cytoplasmic pool of CTLA4 molecules clears over time ($R_c(t) \rightarrow 0$) and reduces by 98% within 2.3 hours (see Fig. 1C, unlabeled cytoplasmic subset). Consequently, the flow of free CTLA4 molecules to the cell surface is reduced and limited to the newly synthesized CTLA4 molecules ($F_{cs}(t) \rightarrow \sigma_i$) (see Fig. 7).

These results suggest that flow of free CTLA4, which controls the rate at which CTLA4 can internalize new ligands, is increasingly compromised by binding of high affinity "non competitive" ligands, such as monoclonal antibodies. The rate of passage from the medium into the cytoplasm for high affinity ligands is highest at the time of exposure to the ligands when there are still many free CTLA4 molecules in the cytoplasm.

Ligand uptake is most efficient at intermediate affinities

To investigate the uptake kinetics of physiological ligands, we employed a ligand uptake model that explicitly considers CTLA4:ligand binding reactions (see Fig. 8). We relaxed the previous assumption in the staining model (Fig. 1A-B)

that ligands are abundantly available in the extracellular environment (assumption A). It is assumed that modeled ligands in the extracellular medium (with concentration $L_p(t)$) react with free surface CTLA4 ($R_p(t)$) with constant on-rate (k_{on}) and off-rate (k_{off}). The complexes ($R_p^*(t)$) can be internalized and degraded by the rate of CTLA4 internalization (k_i) and degradation (δ_c), respectively. Free ligands appear in the cytoplasm ($L_c(t)$) via unbinding of the cytoplasmic complexes ($R_c^*(t)$) to the reactants with the rate $n \times k_{off}$, with $n \leq 1$. We assumed that free ligands cannot bind again to free CTLA4 in the cytoplasm. Since free ligands in the cytoplasm do not interact with other trafficking molecules in the model, the absolute value of their degradation rate does not impact onto extracellular ligand uptake. For simplicity, we assumed the same rate as for the degradation of CTLA4:ligand complexes. Unbound CTLA4 molecules directly join other free cytoplasmic CTLA4 molecules ($R_c(t)$), which subsequently can be recycled (with rate k_r) or degraded (with rate δ_c). The mathematical model is described in Eq. S35 (see *SM - Ligand uptake model*). We performed *in silico* cell culture experiments with a cell count of 10^6 cells/ml. This gives a volume of the extracellular medium per cell (V_γ) equal to 10^{-9} Liters/cell. This setting was kept for all *in silico* experiments.

To investigate the role of ligand binding affinities in the kinetics of ligand uptake, the ligand uptake model in Fig. 8 is solved numerically for ligands with different on-rates (fixed off-rates) or off-rates (fixed on-rates). The time at which half of the initial extracellular ligand concentration is depleted (extracellular ligand half-life) was monitored for different initial ligand concentrations (see Fig. 9A-B). These results indicate how fast modeled ligands can be depleted from the extracellular environment via CTLA4 trafficking.

According to Fig. 9A, the uptake of the extracellular ligands with higher on-rates (higher affinities) is faster. In contrast, this process is optimally fast only for an intermediate range of off-rate values (see Fig. 9B). For low off-rates (high affinity ligands), uptake is not efficient since the recovery of CTLA4 from internalized CTLA4:ligand complex and their subsequent recycling is not efficient. For high off-rates (low affinity ligands), CTLA4:ligand complexes on the cell surface are not stable and complex internalization is limited by complex concentration, which results in an inefficient ligand uptake. We conclude that ligand removal from the medium is monotonic in dependence on on-rates but exhibits a maximum efficiency at intermediate off-rates.

To evaluate the capacity of modeled ligands to bind and reduce free CTLA4 molecules, the minimum number of the free CTLA4 molecules ($R_{p,min}$ and $R_{c,min}$) is obtained during the process of ligand uptake. The degree of reduction from the initial (steady state) value is depicted in Fig. 9C-D and shows that this reduction on the plasma membrane depends on both, extracellular ligand concentration and ligand binding affinity (see Fig. 9C). CTLA4 depletion in the cytoplasm is largely independent of the ligand concentration above 10nM (see Fig.

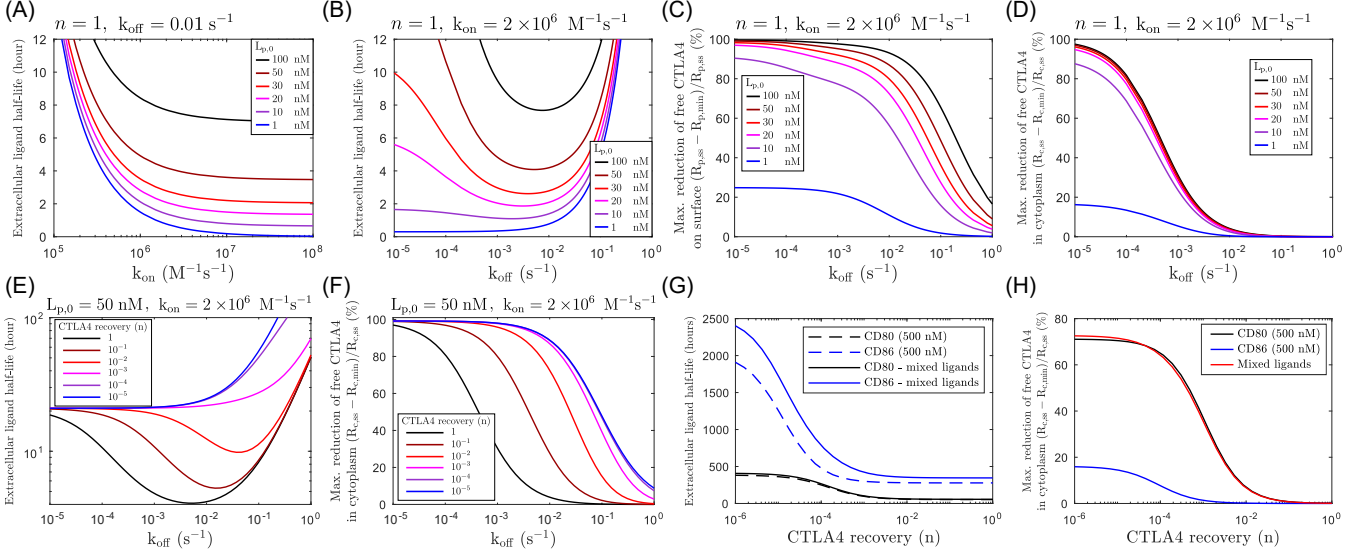


Fig. 9. Extracellular ligand uptake and CTLA4 occupancy. (A,B) The kinetics of ligand uptake is obtained numerically from model S35 for ligands with different binding affinities. Affinities are varied by changing either (A) on-rate (k_{on}), or (B) off-rate (k_{off}) for various initial extracellular ligand concentration. (C,D) The maximum reduction of free CTLA4 by ligand uptake is shown for free CTLA4 (C) on the plasma membrane and (D) in the cytoplasm. (E,F) Same representation as in (B,D) for different CTLA4 recovery rates n . (G,H) Same representation as in (B,D) for an *in silico* mixed-ligand experiment. A two-ligands version of the ligand uptake model S35 was solved with binding affinities of CD80 ($k_{on} = 2.15 \times 10^6 \text{ M}^{-1}\text{s}^{-1}$, $k_{off} = 0.43 \text{ s}^{-1}$) and CD86 ($k_{on} = 1.96 \times 10^6 \text{ M}^{-1}\text{s}^{-1}$, $k_{off} = 5.1 \text{ s}^{-1}$) (40), each with initial ligand concentration of 500 nM. The results are compared with single ligand experiments, with the same initial ligand concentration.

9D). A similar level of reduction in the free cytoplasmic and surface CTLA4 occurs on different values of off-rates, with lower off-rates in the cytoplasm (see Fig. 9C-D). This difference results from a complex interplay of different parameters in the model.

To further investigate the role of the CTLA4 recovery, we varied the factor n in the range $0 < n \leq 1$; lower n corresponds to slower CTLA4 recovery. By reducing the CTLA4 recovery (n), ligand uptake becomes slower (see Fig. 9E), due to a reduced number of free CTLA4 molecules in the cytoplasm (see Fig. 9F). When CTLA4 recovery (n) is highly reduced, no optimal off-rate can be found at which the ligand uptake is maximum. In other words, in the absence of the CTLA4 recovery, ligand removal from the medium is monotonic in dependence on off-rates. Therefore, the process of CTLA4 recovery facilitates uptake of ligands with intermediate off-rates.

The presence of CD80 dominates CTLA4 function A mixture of ligands with different binding affinities results in a binding competition for CTLA4, which may impact the trafficking of CTLA4 and the kinetics of ligand uptake. To investigate the effect of such binding competition for natural ligands (CD80/CD86), we employed an *in silico* mixed ligands experiment by solving a two-ligands version of the model S35. Since the impact of binding affinity/avidity of natural ligands on the rate of CTLA4 recovery ($n \times k_{off}$) is unknown, we obtained ligand uptake kinetics for different values

of the CTLA4 recovery, by changing the value of parameter n ($0 < n \leq 1$).

The reduction of free cytoplasmic CTLA4 is compared between single-ligand and mixed-ligands experiments. Irrespective of the degree of CTLA4 recovery, CD86 uptake is affected by the presence of CD80 molecules, while CD80 removal is almost independent of the presence of CD86 molecules (Fig. 9G). The extent of reduction of free cytoplasmic CTLA4 (for low to intermediate values of n) in the mixed-ligands experiment is similar to the case of exposure to CD80 alone (Fig. 9H). The effect of ligand competition on the kinetics of ligand removal is reduced when the concentration of ligands is low (data not shown). This result suggests that CD86 removal is affected by the presence of CD80, but not vice versa.

Expression of adequate CTLA4 does not guarantee efficient ligand uptake The process of ligand uptake relies on an efficient flow of free CTLA4 to the plasma membrane, provided by synthesis (σ_i) and recycling of free cytoplasmic CTLA4 ($k_r R_c(t)$) (see Eq. 1). Therefore, alterations in the synthesis and recycling processes, as well as a reduced number of free CTLA4 molecules in the cytoplasm can result in inefficient ligand uptake. The steady state number of free cytoplasmic CTLA4 molecules ($R_{c,ss}$) is independent of the recycling process, directly related to the synthesis, and inversely related to the degradation process (see Eq. S2). Therefore, to quantify the impact of impairment in recycling and CTLA4 expression on the kinetic of ligand uptake, we varied separa-

rately the rates of recycling (\hat{k}_r), lysosomal degradation ($\hat{\delta}_l$) and synthesis ($\hat{\sigma}_i$).

Reduced recycling does not significantly alter total free CTLA4 ($\approx 7.5\%$ reduction when recycling is completely blocked, i.e. $\hat{k}_r = 0$). In contrast, increased lysosomal degradation strongly reduces total CTLA4 (compare Fig. 10A and C). Alteration in both processes can slow down the ligand uptake process to a similar extent (compare Fig. 10B and D). This result suggests that a normal process of ligand removal does not only rely on an adequate number of CTLA4 molecules (limited lysosomal degradation), but also on an effective recycling process. In other words, expression of an adequate number of CTLA4 molecules does not guarantee efficient ligand uptake, and efficiency of the recycling process needs to be taken into account.

Alteration in the rate of CTLA4 synthesis directly impacts surface, cytoplasmic, and therefore, total CTLA4 with a similar factor (see Eq. S2). An increased rate of synthesis results in a faster ligand uptake (see Fig. 10E). Depending on the extracellular concentration of the ligands, an extreme increase of the synthesis rate could destroy the existence of the off-rate range where ligand uptake is efficient (see Fig. 10F, $\hat{\sigma}_i = 20 \times \sigma_i$). However, an intermediate increase retains this property. An excess of CTLA4 synthesis reduces the degree of reduction in the free cytoplasmic CTLA4, but has a limited impact on the free surface CTLA4 molecules (see Fig. 10G-H). This result suggests that an increased rate of CTLA4 synthesis can reduce the extent of CTLA4 occupancy in the cytoplasm and its impact on the kinetics of ligand uptake.

Discussion

In the cell-extrinsic regulatory function of CTLA4, an efficient depletion of costimulatory ligands (CD80/CD86) via transendocytosis relies on the trafficking features of CTLA4. In this study, an intracellular trafficking model is constructed by taking into account the essential sub-processes involved in the constitutive trafficking of transmembrane proteins. Starting from a simplistic mathematical model of CTLA4 trafficking, we only added extra complexities when necessary to capture the specifics of different independent experiments used for characterizing the kinetics of CTLA4 molecules. This approach enabled us to carefully estimate all CTLA4 trafficking parameters in the original model (see Table 1), and avoid uncertainties arising from considering a complex model that suffers from unidentifiable parameters. Some aspects of CD28 and CTLA4 signaling have been investigated by mathematical modeling. Using a deterministic model, Jansson et al. (30) considered CD28 and CTLA4 interactions with their natural ligands in immunological synapse in the absence of ligand uptake. More recently, a spatially resolved stochastic model of T-APC interaction has been developed that assumes CTLA4 and ligand internalization without quantitative parameter esti-

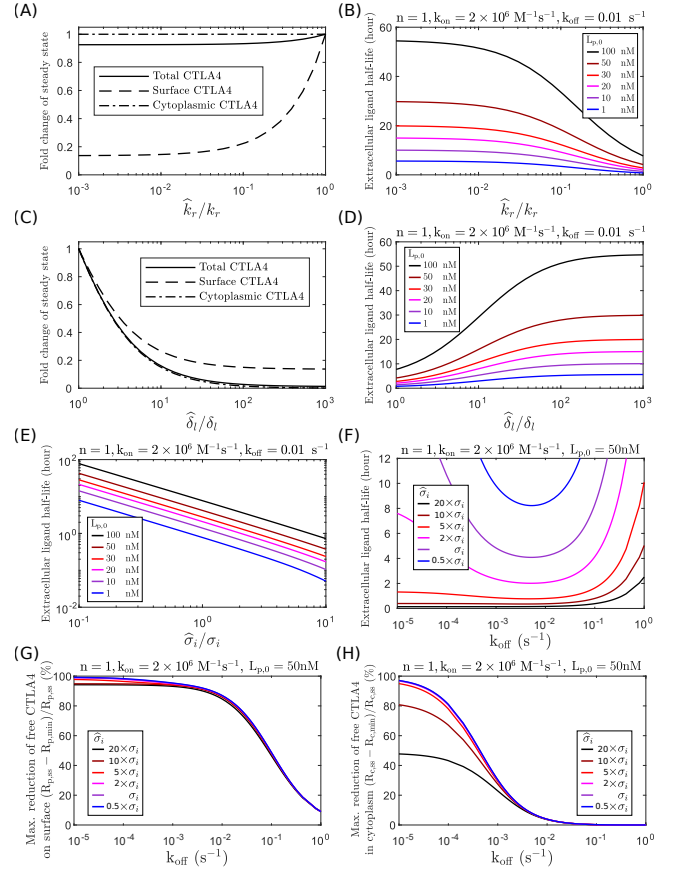


Fig. 10. Alterations in recycling, degradation and synthesis. Impact of alteration in the rate of recycling and degradation on (A,C) the steady state number of free CTLA4 molecules and (B,D) the kinetics of ligand uptake. The fold-change in the steady state number of free CTLA4 molecules by changing the rate of (A) recycling (\hat{k}_r) or (C) lysosomal degradation ($\hat{\delta}_l$), is calculated from Eq. S2. k_r , δ_l and σ_i denote the estimated natural rates for CTLA4 recycling, lysosomal degradation and synthesis, respectively, given in Table 1. The ligand uptake model in Fig. 8 (Eq. S35) is solved numerically with altered rates of (B) recycling (\hat{k}_r), (D) lysosomal degradation ($\hat{\delta}_l$), and (E) synthesis ($\hat{\sigma}_i$) for different initial ligand concentrations ($L_{p,0}$), and the half-life of extracellular ligand concentration is shown for different off-rates. The maximum degree of reduction of free CTLA4 molecules (G) on the cell surface and (H) in the cytoplasm is obtained for different rates of CTLA4 synthesis and off-rates. $R_{p,ss}$ and $R_{c,ss}$ are the steady state number of free CTLA4 molecules in the absence of ligand, and is evaluated for each of the considered synthesis rates.

mation (31). The estimated parameters in our work can inform such theoretical attempts focusing on detailed events during T-APC interactions, where CTLA4 and its quantitatively unique trafficking features are essential.

The analytic solutions derived from the mathematical models revealed the explicit dependencies of experimental measurements on each of the trafficking parameters. For example, these explicit solutions verified that the distribution (Eq. S2)

and the observed kinetics of CTLA4 (Eq. S17, Eq. S21, Eq. S25, Eq. S33 and Eq. S34) are independent of the absolute value for the rate of protein synthesis. Therefore, cells with different steady state levels of CTLA4 synthesis would still exhibit similar CTLA4 behavior. We estimated a synthesis rate of $\approx 10^4$ molecules/min/cell for CHO cells, which is quite high due to the expression on a vector construct. Given that T cells are smaller in size and total number of CTLA4 molecules is lower compared to CHO cells (≈ 38 fold lower MFI in stimulated human CD45RA- Tregs, data not shown), a lower rate of CTLA4 synthesis in T cells is expected and is likely to vary substantially for different cell types and conditions. Nonetheless, our estimated internalization rate of CTLA4 is within the same order of magnitude as transferrin receptor (TfR), a carrier protein of iron-bound transferrin, with 50% of surface TfR being internalized within 5 minutes (32, 33). This is consistent with their uptake by similar AP-2 mechanisms.

Our CHO model combined with the mathematical model provided a set up to establish the relevant parameters of CTLA4 trafficking by which the impact of the parameter variations on CTLA4 biology can be investigated. Whilst we recognize that CHO cells are likely to have differences to primary T cells, they nonetheless provide a starting point for our combined modeling approach. The exact parameter values in T cells will depend on cell type (e.g. naïve or memory Treg), activation state and the T cell stimulus; therefore, values are bound to vary. CTLA4 molecules show an unusual distribution in both CHO and T cells, with a high fraction of total CTLA4 being present in the cytoplasm at equilibrium. The estimated parameters confirmed the expectation that this distribution results from very fast trafficking rates, where the ratio of internalization to recycling rates is high (in the range of ≈ 12 in our cell line). The concepts underpinning our model are largely compatible with the behavior of CTLA4 seen in primary T cells in our experience (26). Moreover these concepts have been used to predict the function of CTLA4 on regulatory T cells (34) as well as measure deficits in CTLA4 function in T cells derived from patients (29, 35). Taken together this suggests that the concepts described here are generally robust and relevant to the behavior of primary T human cells. We have found that this large storage of CTLA4 in the cytoplasm in combination with fast recycling provides a temporary compensation for surface CTLA4 loss when protein synthesis is interrupted (see Fig. 3, and unlabeled surface CTLA4 in Fig. 2C). Physiologically, one can therefore consider that additional CTLA4 molecules can be recruited to the plasma membrane in the absence of new protein synthesis which fits well with the rapid increase in CTLA4 at the immune synapse which precedes new protein synthesis. The rate of CTLA4 molecules newly expressed on the cell surface depends on both CTLA4 synthesis and the number of recycled free CTLA4 molecules (see Eq. S1 and Eq. 1). Together with the speed of internalization ($\ln(2)/k_i = 2.3$ minutes), these processes determine how rapidly antibodies/ligands are re-

moved from the extracellular medium or the opposing cell. According to the model, the flow of free CTLA4 molecules to the plasma membrane is highest at the time of initial exposure to antibodies or ligands and decreases within ≈ 2.3 hours (see Fig. 7). During this period of time, the pool of free cytoplasmic CTLA4 molecules is exhausted and replaced by an antibody labeled pool in the case of high affinity antibodies (see Fig. 1C). In this situation, the rate of antibody removal from the medium is decreased and ultimately limited to the binding of newly synthesized CTLA4 molecules. Viewed in the context of the transendocytosis model, this result suggests that efficient ligand capture may be achieved when CTLA4 expressing T cells remain bound to a single APC for a short duration (less than 2.3 hours). The T cell experiences a period during which the depleted free cytoplasmic CTLA4 is restored and the internalized ligands are degraded. This may limit the efficiency of CTLA4 expressing T cells in removing target molecules from multiple subsequent APCs or the same APC over extended times. In a two-photon imaging study, it was shown that Tregs, which constitutively express CTLA4 (36, 37), make transient interactions with lymph node resident dendritic cells (DC) with an average duration of 3.3 minutes, and up to 40 minutes with migratory activated DCs (38) suggesting rapid depletion by CTLA4 is essential. These measured contact durations, according to the model, would allow for an efficient and persistent removal of co-stimulatory molecules.

The above limitation induced by the depletion of the free cytoplasmic CTLA4 and an increase in bound CTLA4 can be overcome if CTLA4 molecules return to the recycling pool following ligand binding (CTLA4 recovery). Our results show that an optimal affinity must exist at which CTLA4 most efficiently takes up ligands. If affinity is too weak then binding to ligands on the cell surface is compromised. However, the data suggest that if affinity is too high then this may compromise the regeneration of a recycling pool of unbound CTLA4. In this scenario, CTLA4 molecules bound to their target would fail to dissociate from the target following internalization and show delayed re-entry into the pool of free cytosolic CTLA4 available for recycling (see Fig. 8). Given that the CTLA4-ligand off-rate would control the rate of CTLA4 recovery this indicates that the two ligands may differ substantially. On the one hand, a low off-rate due to too high affinity/avidity would limit CTLA4 recovery. On the other hand, a low off-rate increases interaction on the cell surface and, by this increases the probability of transendocytosis. Therefore, a subtle balance between ligand binding reaction and CTLA4 trafficking is needed for maintenance of efficient transendocytosis in a stable CTLA4⁺ T-APC interaction. The model predicts how the kinetics of ligand uptake is altered by variations in binding affinities (Fig. 9) and trafficking parameters (Fig. 10).

Our simulations for ligand removal process aimed to investigate the natural ligands (CD80/CD86) as well as therapeutic

tic ligands that blocks CTLA4 for therapeutic purposes. The therapeutic ligands typically bind CTLA4 with higher affinities than natural ligands which enables their exploitative binding. For example, Ipilimumab ($k_D = 18.2$ nM) and Tremelimumab ($k_D = 5.89$ nM) bind CTLA4 with higher affinity compared to natural ligands ($k_{D,CD86} = 2.6\mu\text{M}$, $k_{D,CD80} = 0.2\mu\text{M}$) (39, 40). A mapping between affinities (off-rates) to the uptake kinetic of physiological ligands in our model should be made with caution due to the factors which cannot be inferred experimentally and the impact of multivalent avidity affecting ligand binding. These processes include recovery of CTLA4 from internalized complexes. In addition to dissociation, other processes are involved in guiding recovered CTLA4 to the recycling endosomes which slow down the CTLA4 recovery. We therefore introduced the parameter n ($n \leq 1$) in the rate of CTLA4 recovery ($n \times k_{\text{off}}$) to account for these uncertainties. By reducing the value of n , we observed the impact of CTLA4 recovery on ligand removal (see Fig. 9E-H). Our results predict a nonlinear relationship between ligand:CTLA4 affinity and extracellular ligand half-life which is not validated experimentally and motivates further experiments.

For modeled ligands with off-rates in the range of CD80/CD86 off-rates, free cytoplasmic CTLA4 is not reduced, irrespective of the ligand concentration (see Fig. 9D for off-rates higher than 10^{-2} (s^{-1}), and Fig. 9H for values of n higher than 10^{-1}). This suggests that the flow of free CTLA4 to the surface is not affected by complex formation with the natural ligand and complex internalization, and, consequently, ligand uptake keeps working at maximum capacity. However, this is based on monomeric affinities, whereas the interaction avidities are unknown. The CD80-CTLA4 interactions are dimer-dimer interactions with the potential for very substantial avidity enhancement (41). In contrast, CD86-CTLA4 interactions appear to be monomeric. Accordingly, this offers the clear possibility that available CTLA4 for recycling may differ substantially between the two ligands (see Fig. 9H for low values of n that would correspond to higher avidities). In this regard it is of considerable interest that our data show that CD80-CTLA4 interactions are dominant over those of CD86, and CD80 affects clearance of CD86, but not vice versa (see Fig. 9G). Although the dominance of CD80 could be readily explained by its high affinity/avidity for CTLA4, our *in silico* results suggest that this dominance could also be partially impacted from the CTLA4 occupancy with CD80 in the cytoplasm and shortage of the recycling free CTLA4. Consistent with this, we have observed experimentally that capture of CD80 largely inhibits uptake of CD86 when both are co-expressed on CHO cells (data not shown). In the context of T cell activation, this would suggest enhanced CD28:CD86 binding and signaling, when CD80 is expressed.

In the context of T-APC interactions, upon cytoskeletal polarization of T cells towards APCs, cytoplasmic CTLA4 is

translocated to the immunological synapse, which may facilitate CTLA4 exocytosis and increase CTLA4 surface density in the quasi two-dimensional interaction face (24, 35). This could result in a significantly higher binding rate of ligands and CTLA4 than in solution.

Lipopolysaccharide-responsive and beige-like anchor protein (LRBA) is an intracellular protein, which colocalizes with CTLA4 in endosomal vesicles. Patients with LRBA mutations exhibit a reduction in CTLA4 expression in the non-activated state (42). However, since CTLA4 is synthesised normally, activation of T cells can still upregulate CTLA4 (29). It has been suggested that the interaction with LRBA in the endosomes rescues CTLA4 from lysosomal degradation, such that LRBA deficiency results in higher degradation and lower recycling of CTLA4 (42, 43). Our model predicted that recycling defects alone cannot account for a significant reduction in the total number of CTLA4 molecules, in contrast to the impact of lysosomal degradation (see Fig. 10A-C). Given that the defect in CTLA4 expression in some patients with LRBA mutation is not very large following activation (29), our *in silico* results suggest that the problem in patients is mainly the need for effective recycling to capture co-stimulatory ligands.

The presented experimentally validated model provides a framework for new insights into the control of immune T cell responses. Having established such a model, important biological questions related to immune regulation and autoimmune disease can be addressed. We have addressed how the two natural ligands CD80 and CD86 with different binding affinities for CTLA4, might have differential impact on CTLA4 biology. We have analyzed the hypothetical impact of biologically relevant changes in parameters affecting synthesis, recycling, ligand affinity and competition revealing insights into behavior that can now be further explored. Moreover, it is already evident that mutations in CTLA4 (44, 45) and most likely in its ligands will occur in the context of immunological diseases. Such mutations may affect the binding affinity with unknown consequences. Accordingly, with additional experimental data it would become possible to predict the impact of such changes on immune function with the help of this model.

Author contributions

M.M.-H., L.S.K.W. and D.M.S. designed research; S.K. developed and analyzed mathematical models; S.K. and J.D.B.H. performed MCMC analysis; B.R., E.W. and N.H. performed experiments; all authors contributed in analyzing the data and writing the paper.

Acknowledgements

S.K. acknowledges the support of the German Federal Ministry of Education and Research (BMBF) for the eMED

project SYSIMIT. B.R. and E.W. were supported by UK Biotechnology and Biological Sciences Research Council (BBSRC). P.A.R. and M.M.-H. were supported by the Human Frontier Science Program (RGP0033/2015). M.M.-H was supported by iMed the Helmholtz Initiative on Personalized Medicine. L.S.K.W. was supported by the Medical Research Council (MRC). N.H. and D.M.S. were supported by Wellcome Trust. J.D.B.H. was supported by the HZI International Graduate School for Infection Research (GS-FIRE). The authors wish to thank Sebastian Binder and Ghazal Montaseri for revising the manuscript. The authors declare no conflicting financial interests.

References

- [1] D. M. Sansom. CD28, CTLA-4 and their ligands: who does what and to whom? *Immunology*, 101(2):169–177, 2000.
- [2] D. J. Lenschow, T. L. Walunas, and J. A. Bluestone. CD28/B7 system of T cell costimulation. *Annu. Rev. Immunol.*, 14:233–258, 1996.
- [3] M. E. Keir and A. H. Sharpe. The B7/CD28 costimulatory family in autoimmunity. *Immunol Rev.*, 204:128–43, 2005.
- [4] P. S. Linsley, W. Brady, L. Grosmaire, A. Aruffo, N. K. Damle, and J. A. Ledbetter. Binding of the B cell activation antigen B7 to CD28 costimulates T cell proliferation and interleukin 2 mRNA accumulation. *J. Exp. Med.*, 173(3):721–730, 1991.
- [5] C. B. Thompson, T. Lindsten, J. A. Ledbetter, S. L. Kunkel, H. A. Young, S. G. Emerson, J. M. Leiden, and C. H. June. CD28 activation pathway regulates the production of multiple T-cell-derived lymphokines/cytokines. *Proc. Natl. Acad. Sci. U. S. A.*, 86(4):1333–7, 1989.
- [6] N. Jain, H. Nguyen, C. Chambers, and J. Kang. Dual function of CTLA-4 in regulatory T cells and conventional T cells to prevent multiorgan autoimmunity. *Proc. Natl. Acad. Sci. U. S. A.*, 107(4):1524–8, 2010.
- [7] E. A. Tivol, F. Borriello, A. N. Schweitzer, W. P. Lynch, J. A. Bluestone, and A. H. Sharpe. Loss of CTLA-4 leads to massive lymphoproliferation and fatal multiorgan tissue destruction, revealing a critical negative regulatory role of CTLA-4. *Immunity*, 3(5):541–547, 1995.
- [8] P. Waterhouse, J. M. Penninger, E. Timms, A. Wakeham, A. Shahinian, K. P. Lee, C. B. Thompson, H. Griesser, and T. W. Mak. Lymphoproliferative disorders with early lethality in mice deficient in *Ctla-4*. *Science*, 270(5238):985–988, 1995.
- [9] T. L. Walunas, D. J. Lenschow, C. Y. Bakker, P. S. Linsley, G. J. Freeman, J. M. Green, C. B. Thompson, and J. A. Bluestone. CTLA-4 can function as a negative regulator of T cell activation. *Immunity*, 1(5):405–13, 1994.
- [10] M. F. Krummel and J. P. Allison. CD28 and CTLA-4 have opposing effects on the response of T cells to stimulation. *J. Exp. Med.*, 182(2):459–65, 1995.
- [11] M. F. Bachmann, P. Waterhouse, D. E. Speiser, K. McKall-Faienza, T. W. Mak, and P. S. Ohashi. Normal responsiveness of CTLA-4-deficient anti-viral cytotoxic T cells. *J. Immunol.*, 160(1):95–100, 1998.
- [12] M. F. Bachmann, G. Köhler, B. Ecabert, T. W. Mak, and M. Kopf. Cutting edge: lymphoproliferative disease in the absence of CTLA-4 is not T cell autonomous. *J. Immunol.*, 163(3):1128–1131, 1999.
- [13] M. F. Bachmann, A. Gallimore, E. Jones, B. Ecabert, H. Acha-Orbea, and M. Kopf. Normal pathogen-specific immune responses mounted by CTLA-4-deficient T cells: a paradigm reconsidered. *Eur. J. Immunol.*, 31(2):450–458, 2001.
- [14] D. Homann, W. Dummer, T. Wolfe, E. Rodrigo, A. N. Theofilopoulos, M. B. Oldstone, and M. G. von Herrath. Lack of intrinsic CTLA-4 expression has minimal effect on regulation of antiviral T-cell immunity. *J. Virol.*, 80(1):270–280, 2006.
- [15] K. Wing, Y. Onishi, P. Prieto-Martin, T. Yamaguchi, M. Miyara, Z. Fehervari, T. Nomura, and S. Sakaguchi. CTLA-4 control over *Foxp3+* regulatory T cell function. *Science*, 322(5899):271–275, 2008.
- [16] O. S. Qureshi, Y. Zheng, K. Nakamura, K. Attridge, C. Manzotti, E. M. Schmidt, J. Baker, L. E. Jeffery, S. Kaur, Z. Briggs, T. Z. Hou, C. E. Futter, G. Anderson, L. S. Walker, and D. M. Sansom. Trans-endocytosis of CD80 and CD86: a molecular basis for the cell-extrinsic function of CTLA-4. *Science*, 332(6029):600–3, 2011.
- [17] L. S. K. Walker and D. M. Sansom. Confusing signals: Recent progress in CTLA-4 biology. *Trends Immunol.*, 36(2):63–70, 2015.
- [18] P. S. Linsley, J. Bradshaw, J. Greene, R. Peach, K. L. Bennett, and R. S. Mittler. Intracellular trafficking of CTLA-4 and focal localization towards sites of TCR engagement. *Immunity*, 4(6):535–43, 1996.
- [19] H. T. Leung, J. Bradshaw, J. S. Cleaveland, and P. S. Linsley. Cytotoxic T lymphocyte-associated molecule-4, a high-avidity receptor for CD80 and CD86, contains an intracellular localization motif in its cytoplasmic tail. *J. Biol. Chem.*, 270(42):25107–25114, 1995.

- [20] T. Shiratori, S. Miyatake, H. Ohno, C. Nakaseko, K. Isono, J. S. Bonifacino, and T. Saito. Tyrosine phosphorylation controls internalization of CTLA-4 by regulating its interaction with clathrin-associated adaptor complex AP-2. *Immunity*, 6(5):583–589, 1997.
- [21] E. Chuang, M. L. Alegre, C. S. Duckett, P. J. Noel, M. G. Vander Heiden, and C. B. Thompson. Interaction of CTLA-4 with the clathrin-associated protein AP50 results in ligand-independent endocytosis that limits cell surface expression. *J. Immunol.*, 159(1):144–151, 1997.
- [22] Y. Zhang and J. P. Allison. Interaction of CTLA-4 with AP50, a clathrin-coated pit adaptor protein. *Proc. Natl. Acad. Sci. USA*, 94(17):9273–9278, 1997.
- [23] H. Schneider, M. Martin, F. A. Agarraberes, L. Yin, I. Rapoport, T. Kirchhausen, and C. E. Rudd. Cytolytic T Lymphocyte-Associated Antigen-4 and the TCR ζ /CD3 Complex, But Not CD28, Interact with Clathrin Adaptor Complexes AP-1 and AP-2. *J. Immunol.*, 163(4):1868–1879, 1999.
- [24] J. G. Egen and J. P. Allison. Cytotoxic T lymphocyte antigen-4 accumulation in the immunological synapse is regulated by TCR signal strength. *Immunity*, 16(1):23–35, 2002.
- [25] K. I. Mead, Y. Zheng, C. N. Manzotti, L. C. Perry, M. K. Liu, F. Burke, D. J. Powner, M. J. Wakelam, and D. M. Sansom. Exocytosis of CTLA-4 is dependent on phospholipase D and ADP ribosylation factor-1 and stimulated during activation of regulatory T cells. *J. Immunol.*, 174(8):4803–11, 2005.
- [26] O. S. Qureshi, S. Kaur, T. Z. Hou, L. E. Jeffery, N. S. Poulter, Z. Briggs, R. Kenefeck, A. K. Willox, S. J. Royle, J. Z. Rappoport, and D. M. Sansom. Constitutive clathrin-mediated endocytosis of CTLA-4 persists during T cell activation. *J. Biol. Chem.*, 287(12):9429–40, 2012.
- [27] T. Iida, H. Ohno, C. Nakaseko, M. Sakuma, M. Takeda-Ezaki, H. Arase, E. Kominami, T. Fujisawa, and T. Saito. Regulation of cell surface expression of CTLA-4 by secretion of CTLA-4-containing lysosomes upon activation of CD4⁺ T cells. *J. Immunol.*, 165(9):5062–5068, 2000.
- [28] M. Catalfamo, X. Tai, T. Karpova, J. McNally, and P. A. Henkart. TcR-induced regulated secretion leads to surface expression of CTLA-4 in CD4⁺CD25⁺ T cells. *Immunology*, 125(1):70–79, 2008.
- [29] T. Z. Hou, N. Verma, J. Wanders, A. Kennedy, B. Soskic, D. Janman, N. Halliday, B. Rowshanravan, A. Worth, W. Qasim, H. Baxendale, H. Stauss, S. Seneviratne, O. Neth, P. Olbrich, S. Hambleton, P. D. Arkwright, S. O. Burns, L. S. Walker, and Sansom D. M. Identifying functional defects in patients with immune dysregulation due to LRBA and CTLA-4 mutations. *Blood*, 129(11):1458–1468, 2017.
- [30] A. Jansson, E. Barnes, P. Klenerman, M. Harlen, P. Sorensen, S. J. Davis, and P. Nilsson. A theoretical framework for quantitative analysis of the molecular basis of costimulation. *J. Immunol.*, 175(3):1575–85, 2005.
- [31] I. P. Suger, J. Das, C. Jayaprakash, and S. C. Sealton. Multiscale Modeling of Complex Formation and CD80 Depletion during Immune Synapse Development. *Biophys J.*, 112(5):997–1009, 2017.
- [32] A. Ciechanover, A.L. Schwartz, A. Dautry-Varsat, and Lodish H.F. Kinetics of internalization and recycling of transferrin and the transferrin receptor in a human hepatoma cell line. Effect of lysosomotropic agents. *J. Biol. Chem.*, 258(16):9681–9689, 1983.
- [33] C. Watts. Rapid endocytosis of the transferrin receptor in the absence of bound transferrin. *J. Cell. Biol.*, 100(2):633–637, 1985.
- [34] T. Z. Hou, O. S. Qureshi, C. J. Wang, J. Baker, S. P. Young, L. S. Walker, and D. M. Sansom. A transendocytosis model of CTLA-4 function predicts its suppressive behavior on regulatory T cells. *J. Immunol.*, 194(5):2148–2159, 2015.
- [35] T. Yokosuka, W. Kobayashi, M. Takamatsu, K. Sakata-Sogawa, H. Zeng, A. Hashimoto-Tane, H. Yagita, M. Tokunaga, and T. Saito. Spatiotemporal basis of CTLA-4 costimulatory molecule-mediated negative regulation of T cell activation. *Immunity*, 33(3):326–339, 2010.
- [36] T. Takahashi, T. Tagami, S. Yamazaki, T. Uede, J. Shimizu, N. Sakaguchi, T. W. Mak, and S. Sakaguchi. Immunologic self-tolerance maintained by CD25(+)CD4(+) regulatory T cells constitutively expressing cytotoxic T lymphocyte-associated antigen 4. *J. Exp. Med.*, 192(2):303–10, 2000.
- [37] S. Read, V. Malmström, and F. Powrie. Cytotoxic T lymphocyte-associated antigen 4 plays an essential role in the function of CD25(+)CD4(+) regulatory cells that control intestinal inflammation. *J. Exp. Med.*, 192(2):295–302, 2000.
- [38] M. P. Matheu, S. Othy, M. L. Greenberg, T. X. Dong, M. Schuijs, K. Deswarte, H. Hammad, B. N. Lambrecht, I. Parker, and M. D. Cahalan. Imaging regulatory T cell dynamics and CTLA4-mediated suppression of T cell priming. *Nat. Commun.*, 6:6219, 2015.

- [39] M. He, Y. Chai, J. Qi, C.W.H. Zhang, Z. Tong, Y. Shi, J. Yan, S. Tan, and G.F. Gao. Remarkably similar CTLA-4 binding properties of therapeutic ipilimumab and tremelimumab antibodies. *Oncotarget*, 8(40):67129–67139, 2017.
- [40] A. V. Collins, D. W. Brodie, R. J. Gilbert, A. Iaboni, R. Manso-Sancho, B. Walse, D. I. Stuart, P. A. van der Merwe, and S. J. Davis. The interaction properties of costimulatory molecules revisited. *Immunity*, 17(2):201–10, 2002.
- [41] S. Ikemizu, R. J. Gilbert, J. A. Fennelly, A. V. Collins, K. Harlos, E. Y. Jones, D. I. Stuart, and S. J. Davis. Structure and dimerization of a soluble form of B7-1. *Immunity*, 12(1):51–60, 2000.
- [42] B. Lo, K. Zhang, W. Lu, L. Zheng, Q. Zhang, C. Kanellopoulou, Y. Zhang, Z. Liu, J. M. Fritz, R. Marsh, A. Husami, D. Kissell, S. Nortman, V. Chaturvedi, H. Haines, L. R. Young, J. Mo, A. H. Filipovich, J. J. Bleesing, P. Mustillo, M. Stephens, C. M. Rueda, C. A. Chougnet, K. Hoebe, J. McElwee, J. D. Hughes, E. Karakoc-Aydiner, H. F. Matthews, S. Price, H. C. Su, V. K. Rao, M. J. Lenardo, and M. B. Jordan. AUTOIMMUNE DISEASE. Patients with LRBA deficiency show CTLA4 loss and immune dysregulation responsive to abatacept therapy. *Science*, 349(6246):436–440, 2015.
- [43] D. M. Sansom. IMMUNOLOGY. Moving CTLA-4 from the trash to recycling. *Science*, 349(6246):377–378, 2015.
- [44] D. Schubert, C. Bode, R. Kenefeck, T. Z. Hou, J. B. Wing, A. Kennedy, A. Bulashevskaya, B. S. Petersen, A. A. Schäffer, B. A. Grüning, S. Unger, N. Frede, U. Baumann, T. Witte, R. E. Schmidt, G. Dueckers, T. Niehues, S. Seneviratne, M. Kanariou, C. Speckmann, S. Ehl, A. Rensing-Ehl, K. Warnatz, M. Rakhmanov, R. Thimme, P. Hasselblatt, F. Emmerich, T. Cathomen, R. Backofen, P. Fisch, M. Seidl, A. May, A. Schmitt-Graeff, S. Ikemizu, U. Salzer, A. Franke, S. Sakaguchi, L. S. Walker, D. M. Sansom, and B. Grimbacher. Autosomal dominant immune dysregulation syndrome in humans with CTLA4 mutations. *Nat. Med.*, 20(12):1410–1416, 2014.
- [45] H. S. Kuehn, W. Ouyang, B. Lo, E. K. Deenick, J. E. Niemela, D. T. Avery, J. N. Schickel, D. Q. Tran, J. Stoddard, Y. Zhang, D. M. Frucht, B. Dumitriu, P. Scheinberg, L. R. Folio, C. A. Frein, S. Price, C. Koh, T. Heller, C. M. Seroogy, A. Huttenlocher, V. K. Rao, H. C. Su, D. Kleiner, L. D. Notarangelo, Y. Rampertaap, K. N. Olivier, J. McElwee, J. Hughes, S. Pittaluga, J. B. Oliveira, E. Meffre, T. A. Fleisher, S. M. Holland, M. J. Lenardo, S. G. Tangye, and G. Uzel. Immune dysregulation in human subjects with heterozygous germline mutations in CTLA4. *Science*, 345(6204):1623–1627, 2014.

Supporting Material (SM)

Ligand-free trafficking model of CTLA4

The CTLA4 trafficking model shown in Fig. 1A can be represented by the following nonhomogeneous linear system of ODEs

$$\dot{R}_c(t) = \underbrace{-k_r R_c(t)}_{\text{recycling}} - \underbrace{\delta_c R_c(t)}_{\text{degradation}} + \underbrace{k_i R_p(t)}_{\text{internalization}}, \quad (\text{S1a})$$

$$\dot{R}_p(t) = k_r R_c(t) - k_i R_p(t) + \underbrace{\sigma_i}_{\text{synthesis}}. \quad (\text{S1b})$$

where $R_c(t)$ and $R_p(t)$ denote the number of CTLA4 molecules in the cytoplasm and on the cell surface, respectively, σ_i denotes the rate of CTLA4 synthesis (number of CTLA4 per minute). k_i , k_r and δ_c are the rates of CTLA4 internalization, recycling and cytosolic degradation, respectively. All variables and parameters represent the value for a single cell (per cell). Over-dots denote time derivatives. The quantities are illustrated in Fig. 1A and explained in the main text in section *CTLA4 trafficking in the absence of ligands*. Steady state (ss) trafficking of CTLA4 is characterized by

$$R_{c,ss} = \frac{\sigma_i}{\delta_c}, \quad R_{p,ss} = \frac{\sigma_i(k_r + \delta_c)}{k_i \delta_c}, \quad \frac{R_{p,ss}}{R_{c,ss}} = \frac{k_r + \delta_c}{k_i}. \quad (\text{S2})$$

Using the estimated parameters given in Table 1, the ratio of surface to cytosolic CTLA4 is ≈ 0.094 . The number of surface CTLA4 are $\approx 9\%$ of the total CTLA4 molecules.

CTLA4 staining model

A typical staining protocol of a protein with natural trafficking could be represented by a nonlinear model schematically illustrated in Fig. S1. In this model, it is assumed that free CTLA4 molecules are synthesized by a constant rate σ_i and directly exocytosed to the plasma membrane ($R_p(t)$). The free surface CTLA4 molecules can bind to labeling antibodies ($L_p(t)$) and form CTLA4:antibody complex ($R_p^*(t)$) which can be detected by flow cytometry or confocal microscopy. The extracellular staining reaction ($R_p + L_p \rightleftharpoons R_p^*$) occurs with a constant binding rate k_L and unbinding rate \widehat{k}_L . Free and labeled CTLA4 molecules on the plasma membrane ($R_p(t)$ and $R_p^*(t)$, respectively) are internalized with constant rates k_i and k_i^* , respectively. Once the labeled CTLA4 molecules are in the cytoplasm ($R_c^*(t)$), free labeling antibodies ($L_c(t)$) appear in the cytoplasm via unbinding of the complex to the reactants, which can further bind to free cytoplasmic CTLA4 molecules $R_c(t)$ ($R_c^* \rightleftharpoons R_c + L_c$). The free and labeled cytoplasmic CTLA4 molecules are recycled to the plasma membrane with constant rates k_r and k_r^* , respectively. Note that in this model, internalization is assumed to be the only pathway

by which labeling antibodies could enter the cell cytoplasm from the extracellular environment. Given these assumptions, the CTLA4 staining model can be described by the following set of ODEs

$$\dot{L}_p(t) = k_L R_p(t) L_p(t) - \widehat{k}_L R_p^*(t), \quad (\text{S3a})$$

$$\dot{R}_c(t) = -(\delta_c + k_r + k_L L_c(t)) R_c(t) + k_i R_p(t) + \widehat{k}_L R_c^*(t), \quad (\text{S3b})$$

$$\dot{R}_p(t) = k_r R_c(t) - (k_L L_p(t) + k_i) R_p(t) + \widehat{k}_L R_p^*(t) + \sigma_i, \quad (\text{S3c})$$

$$\dot{R}_p^*(t) = k_L L_p(t) R_p(t) - (\widehat{k}_L + k_i^*) R_p^*(t) + k_r^* R_c^*(t), \quad (\text{S3d})$$

$$\dot{R}_c^*(t) = k_L L_c(t) R_c(t) + k_i^* R_p^*(t) - (\widehat{k}_L + k_r^* + \delta_c^*) R_c^*(t), \quad (\text{S3e})$$

$$\dot{L}_c(t) = -k_L L_c(t) R_c(t) + \widehat{k}_L R_c^*(t) - \delta_L L_c(t). \quad (\text{S3f})$$

The nonlinearity of this model arises from the forward reaction of extracellular and intracellular CTLA4 labeling.

Reduction of the CTLA4 staining model

We use the following assumptions to reduce the staining model S3: (A) L_p is constant and sufficiently large, (B) k_L is sufficiently larger than other reaction rates, (C) \widehat{k}_L is smaller than the other rates and is approximated to zero for the duration of the experiment, and (D) $\delta_c^* = \delta_c$, $k_r^* = k_r$ and $k_i^* = k_i$. Assumptions (A) and (B) imply that the labeling of the surface CTLA4 molecules ($R_p(t)$) is at quasi steady state. By setting $\dot{R}_p(t) = 0$ in Eq. S3c, we have

$$R_p = \frac{k_r R_c(t) + \widehat{k}_L R_p^*(t) + \sigma_i}{k_L L_p + k_i} \quad (\text{S4})$$

Since the cytoplasmic staining antibody $L_c(t)$ appears during the unbinding process of internalized labeled CTLA4 ($R_c^*(t)$), its value at the starting time of the labeling process ($L_{c,0}$) is zero. Then, by employing assumption (C), we evaluate Eq. S3f with $\widehat{k}_L = 0$,

$$\dot{L}_c(t) = -(k_L R_c(t) + \delta_L) L_c(t). \quad (\text{S5})$$

Therefore, $L_c(t)$ remains at its equilibrium point, i.e.

$$L_c(t) = L_{c,0} = 0. \quad (\text{S6})$$

Next, we substitute Eqs. S4 and S6 in Eq. S3b,

$$\begin{aligned} \dot{R}_c(t) = & -(\delta_c + k_r) R_c(t) + \frac{k_i k_r}{k_L L_p + k_i} R_c(t) \\ & + \frac{k_i \widehat{k}_L}{k_L L_p + k_i} R_p^*(t) + \frac{\sigma_i k_i}{k_L L_p + k_i}. \end{aligned} \quad (\text{S7})$$

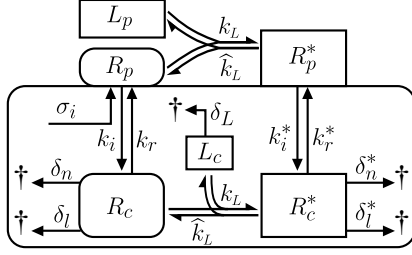


Fig. S1. CTLA4 staining model.

According to assumptions (A) and (B), we extract $k_L L_p \gg k_i k_r$, $k_L L_p \gg k_i \hat{k}_L$ and $k_L L_p \gg \sigma_i k_i$. Therefore, the ratios in Eq. S7 can be approximated to zero, and Eq. S7 can be simplified to

$$\dot{R}_c(t) = -(\delta_c + k_r)R_c(t). \quad (\text{S8})$$

Next, we evaluate Eq. S3d according to Eqs. S4 and S6 and assumptions (C) and (D),

$$\dot{R}_p^*(t) = \frac{k_L L_p}{k_L L_p + k_i} (k_r R_c(t) + \sigma_i) - k_i R_p^*(t) + k_r R_c^*(t). \quad (\text{S9})$$

From assumptions (A) and (B), we extract $k_L L_p \gg k_i$. Therefore, $k_L L_p / (k_L L_p + k_i) \approx 1$, and Eq. S9 can be simplified to

$$\dot{R}_p^*(t) = k_r R_c(t) + \sigma_i - k_i R_p^*(t) + k_r R_c^*(t). \quad (\text{S10})$$

Finally, we evaluate Eq. S3e according to Eqs. S4, S6 and assumptions (C) and (D), and obtain

$$\dot{R}_c^*(t) = k_i R_p^*(t) - (k_r + \delta_c)R_c^*(t). \quad (\text{S11})$$

The simplified model is shown in Fig. 1A-B and reads:

$$\dot{R}_c(t) = -(k_r + \delta_c)R_c(t), \quad (\text{S12a})$$

$$\dot{R}_p(t) = k_r R_c(t) - k_i R_p^*(t) + k_r R_c^*(t) + \sigma_i, \quad (\text{S12b})$$

$$\dot{R}_c^*(t) = k_i R_p^*(t) - (k_r + \delta_c)R_c^*(t), \quad (\text{S12c})$$

One can justify the simplified model in the following way: due to an extremely fast and stable binding of staining antibodies to CTLA4, the unlabeled CTLA4 on the cell surface are labeled instantly, and newly synthesized and recycled unlabeled CTLA4 are stained instantly when reaching the cell surface. Therefore, no unlabeled CTLA4 ($R_p(t)$) exists on the cell surface in the presence of staining antibodies. The source of the surface labeled CTLA4 is recycling of labeled and unlabeled cytoplasmic CTLA4 and synthesis. The labeled cytoplasmic CTLA4 changes by internalization, recycling and degradation.

With initial conditions $R_{c,0} = R_{c,ss}$, $R_{p,0}^* = R_{p,ss}$ (see Eq. S2) and $R_{c,0}^* = 0$, the solution of the model S12 is

$$R_c(t) = \frac{\sigma_i}{\delta_c} e^{-(k_r + \delta_c)t}, \quad (\text{S13a})$$

$$R_p^*(t) = R_{p,0}^* = \frac{\sigma_i(k_r + \delta_c)}{k_i \delta_c}, \quad (\text{S13b})$$

$$R_c^*(t) = \frac{\sigma_i}{\delta_c} (1 - e^{-(k_r + \delta_c)t}) = \frac{\sigma_i}{\delta_c} - R_c(t). \quad (\text{S13c})$$

Note that while the staining antibodies are existing in the medium, the number of stained CTLA4 on the cell surface ($R_p^*(t)$ in Eq. S13b) remains constant. This is resulted from newly synthesized CTLA4 which are continually stained on the cell surface and compensate for the internalization and subsequent degradation of the stained CTLA4 molecules. In experiments with time-limited staining followed by removal of excess antibodies, recycled and newly synthesized molecules are not labeled further. Then, the dynamics of the labeled CTLA4 molecules in Eq. S12 is replaced by

$$\dot{R}_p^*(t) = -k_i R_p^*(t) + k_r R_c^*(t). \quad (\text{S14})$$

CTLA4 internalization model

The theoretical number of initially labeled CTLA4 molecules on the cell surface ($R_{p,0}^*$) is the same as Eq. S2, i.e. $R_{p,0}^* = R_{p,ss}$. After washing, the kinetics of labeled CTLA4 molecules on the plasma membrane follows Eq. S14. From the ODEs in Eqs. S12c and S14, the number of labeled CTLA4 molecules can be obtained as

$$R_p^*(t) = -\frac{k_i + \lambda_2}{\lambda_1 - \lambda_2} R_{p,0}^* e^{\lambda_1 t} + \frac{k_i + \lambda_1}{\lambda_1 - \lambda_2} R_{p,0}^* e^{\lambda_2 t}, \quad (\text{S15a})$$

$$R_c^*(t) = \frac{k_i}{\lambda_1 - \lambda_2} R_{p,0}^* e^{\lambda_1 t} - \frac{k_i}{\lambda_1 - \lambda_2} R_{p,0}^* e^{\lambda_2 t}, \quad (\text{S15b})$$

where $\lambda_{1,2}$ belongs to the set of eigenvalues of the CTLA4 staining model S12,

$$\lambda_{1,2} = \frac{1}{2} \left(-(k_i + k_r + \delta_c) \mp \sqrt{(k_i + k_r + \delta_c)^2 - 4k_i \delta_c} \right). \quad (\text{S16})$$

For the purpose of parameters estimation, the fraction Y_{int} of initially labeled CTLA4 molecules that remained on or recycled to the cell surface is of interest (see Fig. 2A), which is equivalent to

$$Y_{\text{int}}(t) = S_{\text{int}} \frac{R_p^*(t)}{R_{p,0}^*} \quad (\text{S17})$$

where S_{int} is an unknown scaling factor that allows estimation of the initial data point, and is fitted during parameters estimation.

Block of CTLA4 synthesis model

Consider the model S1 with imposing $\sigma_i = 0$ during the presence of CHX. At the moment of adding CHX ($t = 0$), the number of CTLA4 molecules ($R_{p,0}$ and $R_{c,0}$) is equal to the steady states of the model S1, given in Eq. S2. With these initial conditions, the CTLA4 levels in the presence of CHX vary according to the following functions

$$R_p(t) = C_1 e^{\lambda_1 t} + C_2 e^{\lambda_2 t}, \quad (\text{S18a})$$

$$R_c(t) = C_1 \frac{k_i + \lambda_1}{k_r} e^{\lambda_1 t} + C_2 \frac{k_i + \lambda_2}{k_r} e^{\lambda_2 t}, \quad (\text{S18b})$$

where

$$C_1 = \frac{\sigma_i [\lambda_1 \lambda_2 + (k_r + \delta_c) \lambda_2]}{\lambda_1 \lambda_2 (\lambda_2 - \lambda_1)}, \quad (\text{S19})$$

$$C_2 = -\frac{\sigma_i [\lambda_1 \lambda_2 + (k_r + \delta_c) \lambda_1]}{\lambda_1 \lambda_2 (\lambda_2 - \lambda_1)} \quad (\text{S20})$$

are the constant coefficients and $\lambda_{1,2}$ are given in Eq. S16.

The theoretical value that corresponds to the experimental measurement is

$$Y_{\text{CHX}}(t) = \frac{R_p(t) + R_c(t)}{R_{p,0} + R_{c,0}}. \quad (\text{S21})$$

Note that in Eq. S21, the rate of protein synthesis (σ_i) does not appear.

Block of lysosomal degradation

From the solution of the CTLA4 staining model S12 given in Eq. S13, we obtain the number of labeled CTLA4 molecules after 60 minutes on the plasma membrane ($R_{p,60}^*$) and in the cytoplasm ($R_{c,60}^*$). Note that in this stage of the experiment, we have $\delta_c = \delta_l + \delta_n$. After washing cells, labeled CTLA4 molecules change over time according to Eqs. S12c and S14 with the following solutions

$$R_p^*(t) = C_1 e^{\lambda_1 t} + C_2 e^{\lambda_2 t}, \quad (\text{S22a})$$

$$R_c^*(t) = C_1 \frac{k_i + \lambda_1}{k_r} e^{\lambda_1 t} + C_2 \frac{k_i + \lambda_2}{k_r} e^{\lambda_2 t}, \quad (\text{S22b})$$

where

$$C_1 = -R_{c,60}^* \frac{k_r}{\lambda_2 - \lambda_1} + R_{p,60}^* \frac{k_i + \lambda_2}{\lambda_2 - \lambda_1}, \quad (\text{S23})$$

$$C_2 = R_{c,60}^* \frac{k_r}{\lambda_2 - \lambda_1} - R_{p,60}^* \frac{k_i + \lambda_1}{\lambda_2 - \lambda_1}, \quad (\text{S24})$$

are the constant coefficients and the values for $\lambda_{1,2}$ have the same form as in Eq. S16, but with different rates of cytoplasmic degradation (δ_c) reflecting the different experimental condition; in the presence of NH_4Cl in the medium, we have $\delta_c = \delta_n$ whereas in the control experiment $\delta_c = \delta_l + \delta_n$ holds.

Experimentally measured MFI values for the lysosomal-block experiment ($Y_{\text{NH}_4\text{Cl}}(t)$) and the control experiment ($Y_{\text{CTR}}(t)$) are correlated with the subcellular labeled CTLA4 molecules

$$Y_{\text{NH}_4\text{Cl}}(t) = S_{\text{NH}_4\text{Cl}} \frac{R_p^*(t) + R_c^*(t)}{R_{p,60}^* + R_{c,60}^*}, \quad (\text{S25a})$$

$$Y_{\text{CTR}}(t) = S_{\text{CTR}} \frac{R_p^*(t) + R_c^*(t)}{R_{p,60}^* + R_{c,60}^*}. \quad (\text{S25b})$$

Note that in Eqs. S25a and S25b, the rate of cytosolic degradation is different.

CTLA4 recycling model

Following the recycling experiment, the corresponding model is constructed in two steps. This model is illustrated schematically in Fig. S2A-B. During the first step of staining with green primary antibodies, a subset of CTLA4 molecules was labeled at the cell surface and subsequently internalized. The labeled CTLA4 on the plasma membrane and in cytoplasm are represented by $R_p^g(t)$ and $R_c^g(t)$, respectively. From the staining model S12 and steady state solutions in Eqs. S13b and S13c, we obtain the number of green-labeled CTLA4 molecules ($R_{p,60}^g$).

Then in experiment, green-labeled CTLA4 molecules on the cell surface (R_p^{gB}) are blocked on ice, which imposes an initial value of $R_{p,0}^{gB} = R_{p,60}^g$ equal to the number of green-labeled surface CTLA4 molecules after the first staining step. The blocked cytoplasmic pool R_c^{gB} changes from its initial value $R_{c,0}^{gB} = 0$ only after raising the temperature to 37°C .

Next, after washing and raising the temperature, the numbers of red-green labeled CTLA4 molecules on the plasma membrane (R_p^{gr}) and in the cytoplasm (R_c^{gr}) change from their initial values $R_{p,0}^{gr} = R_{c,0}^{gr} = 0$. During this second staining step, the number of CTLA4 molecules in different pools relies on the following dynamical model

$$\dot{R}_p^{gB}(t) = -k_i R_p^{gB}(t) + k_r R_c^{gB}(t), \quad (\text{S26a})$$

$$\dot{R}_c^{gB}(t) = k_i R_p^{gB}(t) - (k_r + \delta_c) R_c^{gB}(t), \quad (\text{S26b})$$

$$\dot{R}_c^g(t) = -(k_r + \delta_c) R_c^g(t), \quad (\text{S26c})$$

$$\dot{R}_p^{gr}(t) = k_r R_c^g(t) - k_i R_p^{gr}(t) + k_r R_c^{gr}(t), \quad (\text{S26d})$$

$$\dot{R}_c^{gr}(t) = k_i R_p^{gr}(t) - (k_r + \delta_c) R_c^{gr}(t). \quad (\text{S26e})$$

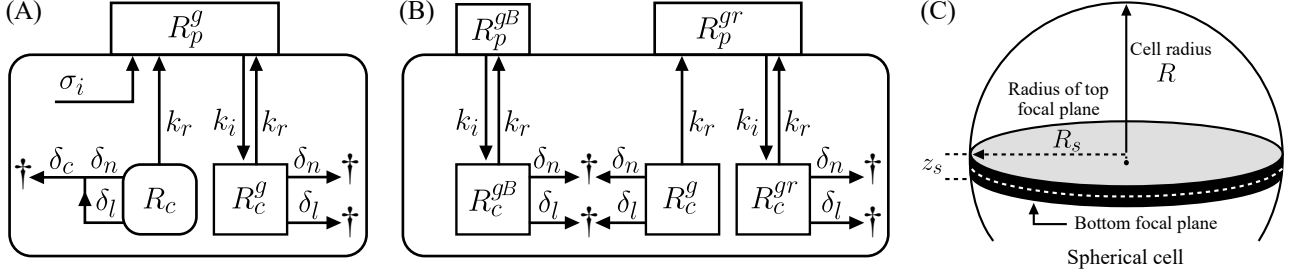


Fig. S2. CTLA4 recycling model. The recycling model is developed for two staining steps. (A) Schematic of the first step staining with Alexa488-conjugated anti-CTLA4 (green). (B) Schematic of the second stage staining with Alexa555-conjugated anti-human IgG secondary antibody (red), during which the recycling green-labeled CTLA4 molecules occurs after initially blocking the green-labeled CTLA4 molecules on plasma membrane (on ice). Note that the number of green-labeled CTLA4 molecules after 1 hour in the first stage is used as the initial conditions for the second stage. (C) Visible area and volume of a spherical cell in confocal microscopy.

Table S1: Parameters associated with experimental data-set and parameter estimation process

Parameter	Description	Dimension	Optimal value ^a	Posterior mean \pm standard deviation ^b
S_{int}	Scaling factor in internalization model; Eq. S17	-	0.937	0.997 ± 0.053
S_{rc}	Scaling factor in recycling model; Eq. S34	-	0.965	1.013 ± 0.054
$S_{\text{NH}_4\text{Cl}}$	Scaling factor in degradation model (+NH ₄ Cl); Eq. S25a	-	1.014	1.009 ± 0.057
S_{CTR}	Scaling factor in degradation model (-NH ₄ Cl); Eq. S25b	-	1.014	0.997 ± 0.056
Δt_{rc}	Shifting time in recycling data; Eq. S34	min	5.61	4.93 ± 0.51
R	Radius of CHO cell	μm	7; fixed	-
z_s	Stack size of confocal microscope	μm	1; fixed	-

^a Optimal values were obtained by differential evolution algorithm.

^b Parameter distributions were obtained by MCMC analysis.

The dynamics of unlabeled CTLA4 molecules is the same as in model S1. The submodel consisting of Eqs. S26a and S26b is equivalent to the internalization experiment, and the submodel consisting of Eqs. S26c-e is equivalent to the homogeneous version of the staining model S12. The solution of model S26 with the given initial conditions is the following

$$R_p^{gB}(t) = R_{p,0}^{gB} \left(-\frac{k_i + \lambda_2}{\lambda_1 - \lambda_2} e^{\lambda_1 t} + \frac{k_i + \lambda_1}{\lambda_1 - \lambda_2} e^{\lambda_2 t} \right), \quad (\text{S27a})$$

$$R_c^{gB}(t) = R_{p,0}^{gB} \left(\frac{k_i}{\lambda_1 - \lambda_2} e^{\lambda_1 t} - \frac{k_i}{\lambda_1 - \lambda_2} e^{\lambda_2 t} \right), \quad (\text{S27b})$$

$$R_c^g(t) = R_{c,60}^g e^{\lambda_3 t}, \quad (\text{S27c})$$

$$R_p^{gr}(t) = R_{c,60}^g \left(\frac{k_r}{\lambda_1 - \lambda_2} e^{\lambda_1 t} - \frac{k_r}{\lambda_1 - \lambda_2} e^{\lambda_2 t} \right), \quad (\text{S27d})$$

$$R_c^{gr}(t) = -R_c^g(t) + R_{c,60}^g \left(\frac{k_i + \lambda_1}{\lambda_1 - \lambda_2} e^{\lambda_1 t} - \frac{k_i + \lambda_2}{\lambda_1 - \lambda_2} e^{\lambda_2 t} \right), \quad (\text{S27e})$$

where $\lambda_{1,2,3}$ are the eigenvalues of staining model S12. The values for $\lambda_{1,2}$ are given in Eq. S16 and $\lambda_3 = -(k_r + \delta_c)$.

All the green- and red-labeled CTLA4 molecules were quantified by confocal microscopy. Note that by confocal microscopy, only a focus plane is visible, and only a fraction of CTLA4 molecules is observable. Therefore, this fraction has to be considered in the theoretical values. In general, by

considering a visible area A_{vis} and a visible volume V_{vis} of a spherical cell with area A and volume V , the following fractions of labeled CTLA4 molecules on the plasma membrane ($R_p^*(t)$) and in the cytoplasm ($R_c^*(t)$) can be observed:

$$R_{p,\text{vis}}^*(t) = \frac{A_{\text{vis}}}{A} R_p^*(t) = \frac{z_s}{2R} R_p^*(t), \quad (\text{S28})$$

$$R_{c,\text{vis}}^*(t) = \frac{V_{\text{vis}}}{V} R_c^*(t) = \frac{z_s(6R_s^2 + z_s^2)}{8R^3} R_c^*(t) \quad (\text{S29})$$

where R is the radius of the spherical cell, z_s is the thickness of the cell slice that is visible by the confocal microscopy and $R_s = \sqrt{R^2 - z_s^2/4}$ is the radius of top focal plane (see Fig. S2C). Theoretical numbers of green- and red-labeled CTLA4 molecules that are visible by confocal microscopy, denoted by $G(t)$ and $R(t)$ respectively, are

$$G(t) = \frac{V_{\text{vis}}}{V} [R_c^{gB}(t) + R_c^g(t) + R_c^{gr}(t)] + \frac{A_{\text{vis}}}{A} [R_p^{gB}(t) + R_p^{gr}(t)], \quad (\text{S30})$$

$$R(t) = \frac{V_{\text{vis}}}{V} R_c^{gr}(t) + \frac{A_{\text{vis}}}{A} R_p^{gr}(t). \quad (\text{S31})$$

These theoretical values are assumed to be proportional to the measured MFI values. For parameter estimation, the same

type of normalization as applied to the experimental data has to be considered for the theoretical values. These normalizations are

$$\bar{G}(t) = \frac{G(t)}{G(t=0)}, \quad (\text{S32})$$

$$Y_{\text{rc,R}}(t) = \bar{R}(t) = \frac{R(t)}{\max(R(t))}. \quad (\text{S33})$$

Note that in Eq. S32, the theoretical and experimental values for $t = 0$ are equal to 1. Therefore, normalization imposes a zero estimation error for the initial data point of the green-labeled pool. To avoid this, we impose a scaling factor S_{rc} which allows an estimation of the initial data point. Furthermore, nonzero value of red fluorescent intensity in Fig. 5A at $t = 0$ indicates a delay between the starting time of the recycling process and the measurement. Therefore, we define a shifting time (Δt_{rc}) in the model. With these considerations, the theoretical value for the green fluorescent measurement to be used for parameter estimation reads

$$Y_{\text{rc,G}}(t) = \bar{G}(t) = S_{\text{rc}} \frac{G(t)}{G(\Delta t_{\text{rc}})}. \quad (\text{S34})$$

Since we considered the time shift in the experimental values and the red fluorescent measurements are normalized to the maximum value but not to the initial data point, the theoretical value S32 does not need any modification and is suitable for parameter estimation. Note that in Eqs. S33 and S34, the rate of protein synthesis (σ_i) does not appear. The fitting result is shown in Fig. 5A.

Ligand uptake model

The ligand uptake model depicted in Fig. 8 reads:

$$\dot{R}_p = k_r R_c(t) - k_i R_p(t) + \sigma_i - k_{\text{on}} L_p(t) R_p(t) + k_{\text{off}} R_p^*(t), \quad (\text{S35a})$$

$$\dot{R}_c = -(k_r + \delta_c) R_c(t) + k_i R_p(t) + n k_{\text{off}} R_c^*(t), \quad (\text{S35b})$$

$$\dot{L}_p = (N_{\text{av}} V_\gamma)^{-1} (-k_{\text{on}} R_p(t) L_p(t) + k_{\text{off}} R_p^*(t)), \quad (\text{S35c})$$

$$\dot{R}_p^* = k_{\text{on}} L_p(t) R_p(t) - (k_i + k_{\text{off}}) R_p^*(t) + k_r R_c^*, \quad (\text{S35d})$$

$$\dot{R}_c^* = k_i R_p^*(t) - (k_r + \delta_c) R_c^*(t) - n k_{\text{off}} R_c^*(t), \quad (\text{S35e})$$

$$\dot{L}_c = n k_{\text{off}} R_c^*(t) - \delta_c L_c(t). \quad (\text{S35f})$$

The quantities are explained in the main text in section *Ligand uptake is most efficient at intermediate affinities*. N_{av} is Avogadro's number and V_γ is the volume of the extracellular medium per cell.

Parameter estimation

The ligand-independent CTLA4 trafficking model in its simplest form in Eq. S1 has 5 unknown parameters. There are 5

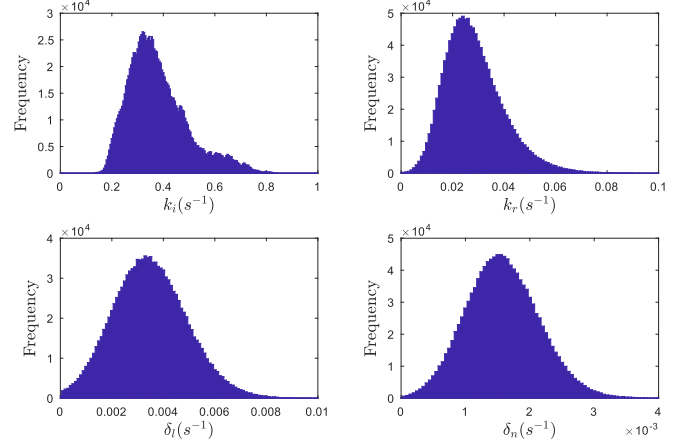


Fig. S3. Posteriori distributions of the model parameters.

additional parameters that are concerned with the types of experimental protocols, and aimed to handle uncertainties. The list of parameters and associated dimensions are given in Table 1. In order to find an optimal parameters set that fits the modeling results to the experimental observations, the following cost (objective) function $E(\theta)$ is minimized

$$E(\theta) = \frac{1}{m} \sum_{k=1}^m \left(\frac{1}{d_k} \sum_{l=1}^{d_k} \left(\frac{\hat{Y}_{kl} - Y_k(\theta, t_l)}{\hat{Y}_{k,\text{max}}} \right)^2 \right), \quad (\text{S36})$$

where \hat{Y}_{kl} is the observed value from k -th experiment at time $t = t_l$ and $Y_k(\theta, t_l)$ is corresponding theoretical value obtained from the model with parameter set θ . d_k is the number of data points in k -th experiment, $\hat{Y}_{k,\text{max}}$ is the maximum observed experimental value in k -th experiment, and m is the number of independent experiments. We used a differential evolution algorithm to minimize the cost function in Eq. S36. The estimated parameter values are given in Table 1 and S1.

Markov chain Monte Carlo analysis

In order to estimate the parameter confidence interval from a Posteriori distribution, Bayesian inference approach by means of Markov chain Monte Carlo (MCMC) was employed. Confidence intervals are calculated following standard Metropolis-Hasting algorithm, assuming a normal error distribution given the set of experimental data. Five millions posterior sample were generated where 75% of it was burn-in. The posteriori means and standard deviations are presented in the Table (1). The optimal value of the CTLA4 trafficking parameters obtained by the differential evolution algorithm are located within one standard error of estimated posterior distribution. These distributions are shown in Fig. S3.

Estimating the rate of protein synthesis

The rate of protein synthesis could not be determined because the models were based on relative counts independent of the CTLA4 synthesis rate. From the model in Fig. 1A we know that CTLA4 synthesis is related to absolute counts of CTLA4. Therefore, we did a molecular counting experiment (see *Materials and methods - CTLA4 molecular counting*). For a typical virally transduced CHO cell line, we estimated $\approx (2.88 \pm 0.126) \times 10^6$ cellular CTLA4-WT per CHO cell, which reflects the total steady state number of CTLA4 molecules. By using this value and the fitted rates of internalization, recycling and degradation, we obtained the rate of protein synthesis from Eq. S2, given in Table 1. We calculated the confidence bound for the rate of synthesis using the Eq. S2, given the confidence bounds of other trafficking parameters from MCMC analysis and variations in the measured total CTLA4 molecules.